

# The Role of Collective Neutrino Flavor Oscillations in Core-Collapse Supernova Shock Revival

Basudeb Dasgupta,<sup>1</sup> Evan P. O'Connor,<sup>2</sup> and Christian D. Ott<sup>2</sup>

<sup>1</sup>CCAPP, The Ohio State University, 191 W. Woodruff Avenue, Columbus, OH 43210, USA

<sup>2</sup>TAPIR, California Institute of Technology, MC 350-17, 1200 E. California Blvd., Pasadena, CA 91125, USA

(Dated: 15 September, 2011)

We explore the effects of collective neutrino flavor oscillations due to neutrino-neutrino interactions on the neutrino heating behind a stalled core-collapse supernova shock. We carry out axisymmetric (2D) radiation-hydrodynamic core-collapse supernova simulations, tracking the first 400 ms of the post-core-bounce evolution in  $11.2-M_{\odot}$  and  $15-M_{\odot}$  progenitor stars. Using inputs from these 2D simulations, we perform neutrino flavor oscillation calculations in multi-energy single-angle and multi-angle single-energy approximations. Our results show that flavor conversions do not set in until close to or outside the stalled shock, enhancing heating by not more than a few percent in the most optimistic case. Consequently, we conclude that the postbounce pre-explosion dynamics of standard core-collapse supernovae remains unaffected by neutrino oscillations. Multi-angle effects in regions of high electron density can further inhibit collective oscillations, strengthening our conclusion.

PACS numbers: 14.60.Pq, 97.60.Bw

## I. INTRODUCTION

Stars with a zero-age main-sequence (ZAMS) mass greater than  $\sim(8-10)-M_{\odot}$  undergo core collapse at the end of their lives. When the inner core reaches nuclear density, the stiffening of the nuclear equation of state (EOS) induces core bounce, launching a strong shock wave that slams into the still infalling outer core. Created at a mass coordinate of  $\sim 0.5-M_{\odot}$  and endowed with the kinetic energy from infall, the shock initially moves out rapidly in mass and radius, but dissociation of heavy infalling nuclei and neutrino losses from neutronization and thermal processes in the hot region behind the shock sap its energy. As a result, the shock soon succumbs to the ram pressure of the outer core and stalls at a radius of  $\sim(100-200)$  km.

Finding the mechanism that robustly revives the stalled shock to blow up a massive star in a core-collapse supernova has been the primary objective of core-collapse supernova theory for decades, but so far success has been limited. The *neutrino mechanism* [1, 2], based on the net deposition of neutrino energy by charged-current absorption in the semi-transparent *gain* region below the shock, has been shown by radiation-hydrodynamics simulations to work in its purest, spherically-symmetric (1D) form only in the lowest-mass massive stars with oxygen-neon cores [3–5] and the most accurate 1D simulations fail to explode more massive stars [6, 7]. In axisymmetry (2D), neutrino-driven convection and the standing-accretion-shock instability (SASI, *e.g.*, [8–10]) increase the efficacy of the neutrino mechanism (by enhancing heating [11–13] or reducing cooling by neutrinos [14]). Neutrino-driven explosions in 2D simulations have been reported [13, 15, 16], though only in models using the softest variant of the Lattimer-Swesty EOS [17], which is disfavored by the recent discovery of a  $2-M_{\odot}$  neutron star [18], but leads to a compact protoneutron star (PNS) and a hard neutrino spectrum [13, 19], favorable for heating due to the  $\epsilon_{\nu}^2$  dependence of the neutrino absorption cross section.

Other multi-dimensional phenomena have led to proposals of alternatives to the neutrino mechanism: Rapid rotation in combination with rotational magnetic field amplification can lead to magnetorotational explosions with bipolar morphology [20–23]. But rapid core rotation may be present only in a small fraction of all massive stars [24, 25], ruling out this *magnetorotational mechanism* for the garden-variety core-collapse supernova. Burrows *et al.* [26, 27] proposed an *acoustic mechanism* in which non-linear PNS oscillations, driven by turbulence and accretion downstreams, emit sound waves into the region behind the shock that steepen to secondary shocks, injecting heat and reviving the stalled shock. The acoustic mechanism leads to perhaps too late, too weak explosions and bleeding of PNS oscillation power to numerically unresolved daughter modes may diminish its relevance in nature [28].

Exploratory 3D simulations [29, 30] are suggestive of the possibility that the additional degree of freedom over 2D and the physical nature of turbulence in 3D could render the neutrino mechanism robust. But full 3D neutrino radiation-hydrodynamics simulations must be awaited before 3D can be declared the missing piece in the core-collapse supernova puzzle.

The marginality of the various proposed mechanisms combined with nature's robust ability to produce explosions in massive stars up to at least  $\sim 20-M_{\odot}$  [31, 32] makes one wonder: *Is there important physics missing from core-collapse supernova models?* With the current standard set of physics included in models, we might, for example, miss an early hadron-quark phase transition in the PNS, leading to a second collapse and bounce and a second shock wave that revives the first. This possibility was proposed by [33, 34], but requires a soft hadronic EOS that has now been ruled out.

In this article, we consider new physics that has not previously been included in the core-collapse supernova problem: self-induced collective neutrino flavor oscillations. Neutrino oscillations have long been known to

occur in vacuum (*e.g.*, [35]) and in matter, mediated by neutrino-electron scattering (via the Mikheyev-Smirnov-Wolfenstein (MSW) effect, [36, 37]). Less appreciated, until recently, has been the possibility of oscillations occurring due to neutrino-neutrino forward scattering in regions of high neutrino number density. This self-induced oscillation process was first discussed in [38] and then explored in a series of papers [39–46]. Thereafter, following the simulations of Duan *et al.* [47, 48], it has received much attention recently as a process occurring in the core-collapse supernova environment and leading to flavor conversions of neutrinos and antineutrinos of almost all energies (*e.g.*, [49–68]. Also see the review [69]).

The most intriguing result of these so-called “collective oscillations” (flavor conversions take place collectively over all energies) is an almost complete exchange of electron neutrino ( $\nu_e$ ) and antineutrino ( $\bar{\nu}_e$ ) spectra with the spectra of the heavy-lepton neutrinos and antineutrinos  $\nu_x \in \{\nu_\mu, \nu_\tau, \bar{\nu}_\mu, \bar{\nu}_\tau\}$ . The  $\nu_x$ , due to the absence of muons and taus, do not interact via charged-current processes in core-collapse supernovae. They are created by thermal processes in the PNS core and decouple from matter at smaller radii and higher temperatures than  $\nu_e$  and  $\bar{\nu}_e$ . Hence, the initial  $\nu_x$  spectra are much harder. Due to the  $\epsilon_\nu^2$  dependence of the charged-current absorption cross section, a swap of  $\nu_x$  and  $\nu_e/\bar{\nu}_e$  spectra would dramatically enhance neutrino heating and may be the crucial ingredient missing in core-collapse supernova models, provided the swap occurs at sufficiently small radii in the region behind the shock to boost net heating. This is indeed the recent result obtained by Suwa *et al.* [70], where a neutrino conversion radii was assumed at a radius of 100 km.

Fuller *et al.* [71] were the first to propose increased heating due to neutrino oscillations, but their MSW resonance based oscillation mechanism required a large neutrino mass of  $\sim (10 - 100)$  eV for one of the active neutrinos. Akhmedov *et al.* [72] put forth a similar proposal, but both are now ruled out by stringent constraints on neutrino masses (*e.g.*, [73]).

Self-induced collective neutrino oscillations, on the other hand, do not require large neutrino masses, are a rather straightforward consequence of the Standard Model of particle physics, and may, in principle, occur in both the inverted and the normal neutrino mass hierarchy [60]. In this work, we study their relevance for the core-collapse supernova mechanism by calculating approximate analytic and detailed numerical estimates for the radii at which collective oscillations set in and could influence neutrino heating. We base these calculations on neutrino radiation fields from 2D neutrino radiation-hydrodynamic simulations of the postbounce core-collapse supernova evolution in  $11.2-M_\odot$  and  $15-M_\odot$  progenitor stars, representative of the progenitors of standard Type-II supernovae.

We find that the calculated oscillation radii, while reaching average shock radii, do not penetrate deeply into the heating region. Large shock excursions due to

the SASI reach and surpass the radius at which oscillations set in, but the region in which the vast majority of net heating occurs remains always at least  $\sim 100$  km below the oscillation radius, even in the low-mass  $11.2-M_\odot$  progenitor. Recent results of Chakraborty *et al.* [74, 75], obtained on the basis of 1D simulations, show the suppression of collective oscillations by very high electron number density in dense matter. In our 2D models, we find that such a suppression may be significantly weaker than reported by Chakraborty *et al.*. Nonetheless, the flavor conversion still happens too far out in the supernova, and we conclude that collective neutrino oscillations do not have a significant effect on the explosion mechanism of core-collapse supernovae in progenitors in and above the explored mass range.

The structure of this article is as follows. In Section II, we review neutrino heating in core-collapse supernovae and in Section III, we introduce collective neutrino oscillations and present an approximate analytic prescription that can be used to determine the radius at which neutrinos will begin to collectively oscillate. In Section IV, we go on to discuss our 2D radiation-hydrodynamic postbounce core-collapse supernova simulations and contrast the evolutions of their characteristic radii with the analytic estimates and detailed numerical results for the oscillation radius. This allows us to ascertain the importance of collective neutrino oscillations for shock revival. In Section V, we summarize our results and conclude.

## II. NEUTRINO HEATING IN CORE-COLLAPSE SUPERNOVAE

To elucidate the basics of the neutrino mechanism, we make a number of simplifying assumptions, which we lay out in the following. We assume a spherically symmetric mass distribution and expect neutrinos to stream freely outside their energy-averaged neutrinospheres. We define the neutrinosphere radii for each neutrino species via a Rosseland mean neutrino optical depth,

$$\tau_{\text{RM},\nu_i}(r) = \int_r^\infty \left( \frac{\int_0^\infty J_{\nu_i}/\kappa_{\nu_i} d\epsilon}{\int_0^\infty J_{\nu_i} d\epsilon} \right)^{-1} dr'. \quad (1)$$

and set the neutrinosphere radius  $R_{\nu_i} = R(\tau_{\text{RM},\nu_i} = 2/3)$ . In this expression for the energy-averaged optical depth,  $\kappa_{\nu_i}$  is the sum of the absorption and scattering opacities, and  $J_{\nu_i}$  is the  $\nu_i$  energy density.

The energy-dependent optical depth is a quadratic function of the neutrino energy, the energy-dependent neutrinospheres move outward with neutrino energy (cf. Fig. 13 of [76]). The energy-averaged variant of the optical depth that we use produces a neutrinosphere that matches rather well the radius of the neutrinosphere of the average neutrino energy for each species. In the following, we will consider only the  $\nu_e$  neutrinosphere radius  $R_{\nu_e}$ , since  $\nu_e$  decouple from matter furthest out, followed first by  $\bar{\nu}_e$ , then by  $\nu_x$ . The  $\nu_x$  are not involved

in charged-current interactions, hence have the largest mean free path. The  $\bar{\nu}_e$  interact with the less abundant proton and, hence, also have a greater mean free path than the  $\nu_e$ . This decoupling hierarchy is also present in the mean and mean-squared neutrino energies, giving  $\langle \epsilon_{\nu_x} \rangle > \langle \epsilon_{\bar{\nu}_e} \rangle > \langle \epsilon_{\nu_e} \rangle$  and  $\langle \epsilon_{\nu_x}^2 \rangle > \langle \epsilon_{\bar{\nu}_e}^2 \rangle > \langle \epsilon_{\nu_e}^2 \rangle$ , reflecting the fact that the least interacting neutrino decouples at the smallest radius and the highest matter temperature. Typical values for the mean neutrino energies,  $\langle \epsilon_{\nu_i} \rangle$ , are  $\sim (10 - 15)$  MeV for  $\nu_e$ , and  $\bar{\nu}_e$  and  $\sim (15 - 20)$  MeV for  $\nu_x$  (see, *e.g.*, [19, 77, 78]). In the very early postbounce phase of a core-collapse supernova,  $R_{\nu_e}$  is typically around  $\sim (70 - 80)$  km, reaching  $\sim (30 - 40)$  km within  $(200 - 300)$  ms of core bounce.

We make the assumption that beyond our nominal neutrinosphere  $R_{\nu_e}$ , the radiation fields of all neutrinos are freely streaming with a luminosity  $\mathcal{L}_{\nu_i}$ , an average energy of  $\langle \epsilon_{\nu_i} \rangle$ , a mean squared energy of  $\langle \epsilon_{\nu_i}^2 \rangle$ , and a total *number luminosity* of  $\mathcal{N}_{\nu_i} = 4\pi R_{\nu_e}^2 \Phi_{\nu_i}$ , where  $\Phi_{\nu_i}$  is the neutrino number flux of species  $i$  at radius  $R_{\nu_e}$ . We normalize the spectral neutrino distribution function  $d\Phi_{\nu_i}/d\epsilon$  at the  $\nu_e$  neutrinosphere according to  $4\pi R_{\nu_e}^2 \int_0^\infty d\epsilon d\Phi_{\nu_i}/d\epsilon = 4\pi R_{\nu_e}^2 \Phi_{\nu_i}$ . The neutrino energy distribution function is then simply  $\epsilon d\Phi_{\nu_i}/d\epsilon$ .

Outside of  $R_{\nu_e}$ , conditions arise where absorption of  $\nu_e$  and  $\bar{\nu}_e$  via charged-current interactions with neutrons and protons inject more energy into the matter than is lost due to thermal emission and electron and positron capture on neutrons and protons. This is the case in the *gain region* [79], which, in our simplified 1D picture, extends from the gain radius  $R_g$ , where neutrino heating balances cooling, to the shock radius  $R_s$ . Typical values of  $R_g$  and  $R_s$  during the accretion phase of core-collapse supernovae are  $\sim 100$  km, and  $\sim 200$  km, respectively [12, 13, 77, 80].

In the gain region, the heating due to the charged-current neutrino-matter interactions is given by the absorption cross section  $\sigma_{\nu_i}(\epsilon_{\nu_i})$  convolved with the spectral energy fluxes of both  $\nu_e$ s and  $\bar{\nu}_e$ s incident on the gain region from below,

$$\mathcal{H} = \sum_{\nu_e, \bar{\nu}_e} \int_{r_g}^{r_s} dr 4\pi r^2 n_i \int_0^\infty d\epsilon \sigma_{\nu_i}(\epsilon) \frac{\epsilon d\Phi_{\nu_i}}{d\epsilon}, \quad (2)$$

where  $n_i$  is the local number density of nucleons relevant for interactions with neutrino species  $i$ . For Eq. (2), we approximate  $\sigma_{\nu_i}(\epsilon) = \sigma_0(1 + 3g_A^2)/(4m_e^2 c^4) \times \epsilon^2 = \hat{\sigma}\epsilon^2$ , where  $\sigma_0 \sim 1.76 \times 10^{-44} \text{ cm}^2$  is the reference weak interaction cross section, and  $g_A$  is the axial-vector coupling constant. Note that the units of  $\hat{\sigma}$  are  $\text{cm}^2/\text{MeV}^2$ . This approximation of the neutrino absorption cross section, in combination with our free-streaming assumption, leads to a gross heating rate,

$$\begin{aligned} \mathcal{H} &\sim \sum_{\nu_i} \hat{\sigma} \langle \epsilon_{\nu_i}^2 \rangle \mathcal{L}_{\nu_i} \int_{R_g}^{R_s} dr n_i \\ &\sim \hat{\sigma} [\langle \epsilon_{\nu_e}^2 \rangle \mathcal{L}_{\nu_e} c_N + \langle \epsilon_{\bar{\nu}_e}^2 \rangle \mathcal{L}_{\bar{\nu}_e} c_P], \end{aligned} \quad (3)$$

where  $c_N$  and  $c_P$  are the target nucleon column densities (in  $\#/\text{cm}^2$ ) for  $\nu_e$  and  $\bar{\nu}_e$ , respectively. Note that  $\mathcal{L}_{\nu_i}$  and  $\langle \epsilon_{\nu_i}^2 \rangle$  will typically vary somewhat across the gain region. We neglect this variation for simplicity. Eq. (3) gives the integrated gross heating rate,  $\mathcal{H}$ , but it is important to note that the majority of the heating occurs very near the gain radius due to the strong dependence of the rest-mass density on radius,  $\rho \propto r^{-3}$  (as pointed out by [79] and seen in simulations. See, *e.g.*, Fig. 16 of [77], and Fig. 6 of this work). Also, while neutrino heating dominates over cooling in the gain region, the latter is still significant and must not be neglected. The net heating rate (heating minus cooling) is estimated by Janka [79] to be  $\mathcal{H}_{\text{net}} = \mathcal{H} - \mathcal{C} \approx \mathcal{H}/2$ , which is in rough agreement with what one finds in simulations.

The main take-away message from this section is that the heating rate  $\mathcal{H}$  depends on the  $\nu_e$  and  $\bar{\nu}_e$  spectral fluxes as

$$\mathcal{H} \propto \sum_{\nu_i = \nu_e, \bar{\nu}_e} \mathcal{L}_{\nu_i} \langle \epsilon_{\nu_i}^2 \rangle. \quad (4)$$

Our aim in this study is to explore if flavor conversions due to collective neutrino oscillations can increase the quantity  $\mathcal{L}_{\nu_e, \bar{\nu}_e} \langle \epsilon_{\nu_e, \bar{\nu}_e}^2 \rangle$  to boost the heating mechanism. There are two aspects to this question – (i) What is the typical degree of flavor conversion? (ii) Does this flavor conversion take place at sufficiently small radii to have a significant effect on the total neutrino heating? To address these questions, we discuss collective oscillations in the next section.

### III. COLLECTIVE NEUTRINO FLAVOR CONVERSION

#### A. Equations of Motion

Neutrinos with masses  $m_1, m_2, m_3$  are related to three flavor states  $\nu_e, \nu_\mu, \nu_\tau$ . These flavor states oscillate from one to another as a function of time, depending on the mass-square differences  $\Delta m_{ij}^2 = m_j^2 - m_i^2$  and mixing angles  $\theta_{ij}$ , where the indices run over  $(1, 2, 3)$ . For an introduction to neutrino oscillation physics, see *e.g.*, Chapter 3 of [81]. As is usual in particle physics, we will use units in which the speed of light  $c$  and Planck's constant  $\hbar$  are equal to 1.

In the core-collapse supernova context, a two neutrino flavor approximation is often appropriate because  $\Delta m_{21}^2 \ll |\Delta m_{31}^2|$  and  $\theta_{13} \ll 1$ . In that case, the oscillations are primarily between  $\nu_e$  and the linear combination  $(\nu_\mu - \nu_\tau)/\sqrt{2}$ , while the other linear combination is decoupled from the system. Our numerical results have been obtained with a full three-flavor code. The  $\nu_e \leftrightarrow \nu_x$  and  $\bar{\nu}_e \leftrightarrow \nu_x$  oscillations are governed by  $\Delta m_{\text{atm}}^2 \approx \Delta m_{31}^2$  (the subscript “atm” is used, because this quantity determines the oscillations of neutrinos created in the atmosphere) and the mixing angle  $\theta_{13}$ . We take the absolute value of  $\Delta m_{\text{atm}}^2$  to be  $2.6 \times 10^{-3} \text{ eV}^2$ , close to

the best fit of experimental data [82], while the sign is not known. We will use a benchmark value of  $\theta_{13} = 0.001$ , consistent with the upper limit  $\sin^2 \theta_{13} < 0.035$  [82].

Neutrino oscillations can alter the flux differences  $d\Phi_{\nu_e}/d\epsilon - d\Phi_{\bar{\nu}_e}/d\epsilon$  and  $d\Phi_{\nu_e}/d\epsilon - d\Phi_{\nu_x}/d\epsilon$  at a given energy  $\epsilon$  by a polarization vector  $\mathbf{P}$  and  $\bar{\mathbf{P}}$  in a three-dimensional flavor space, as in [49]. At the neutrinosphere, all neutrinos are emitted as flavor states. Thus the initial polarization vectors are aligned with the  $z$ -direction

$$\mathbf{P}(\epsilon) = \frac{d\Phi_{\nu_e}/d\epsilon - d\Phi_{\nu_x}/d\epsilon}{\Phi_{\nu_e} + \Phi_{\bar{\nu}_e} + 4\Phi_{\nu_x}} \hat{z}, \quad (5)$$

$$\bar{\mathbf{P}}(\epsilon) = \frac{d\Phi_{\bar{\nu}_e}/d\epsilon - d\Phi_{\nu_x}/d\epsilon}{\Phi_{\nu_e} + \Phi_{\bar{\nu}_e} + 4\Phi_{\nu_x}} \hat{z}, \quad (6)$$

where a vertically upward vector represents a  $\nu_e$  (or  $\bar{\nu}_e$ ) excess and a downward vector shows a  $\nu_x$  excess. When the fluxes of  $\nu_e$  (or  $\bar{\nu}_e$ ) and  $\nu_x$  are equal, the polarization vector vanishes. Other directions represent states that are coherent superpositions of the two pure states which will be generated by flavor oscillations.

In the treatment of neutrino oscillations it is important to consider the angle  $\vartheta_{R_{\nu_e}}$  at which neutrinos are emitted from the neutrinosphere at  $R_{\nu_e}$ . We will therefore attach a label  $u$  to polarization vectors signifying the direction of emission, *i.e.*,  $\mathbf{P}(\epsilon, u)$ , where  $u = \sin^2 \vartheta_{R_{\nu_e}}$ . Of course,  $\int_0^1 du \mathbf{P}(\epsilon, u) = \mathbf{P}(\epsilon)$ , and similarly for antineutrinos.

In vacuum, the  $\nu_e$  (or  $\bar{\nu}_e$ ) oscillate to  $\nu_x$  and back with a frequency [35]

$$\omega(\epsilon) = \frac{|\Delta m_{\text{atm}}^2|}{2\epsilon}, \quad (7)$$

$$= 0.65 \text{ km}^{-1} \times \left[ \frac{10 \text{ MeV}}{\epsilon} \right], \quad (8)$$

solely under the action of neutrino masses and mixing. The vacuum Hamiltonian is represented by a vector  $\omega(\epsilon)\mathbf{B}$  with  $\mathbf{B} = \mp(\sin 2\theta_{13}, 0, \cos 2\theta_{13})$  where the minus sign applies for normal neutrino mass hierarchy ( $\Delta m_{\text{atm}}^2 > 0$ ) and the plus sign for inverted neutrino mass hierarchy ( $\Delta m_{\text{atm}}^2 < 0$ ).

In the core-collapse supernova environment there are additional sources of flavor oscillation, *i.e.*, weak inter-

actions with the stellar material, and weak interactions between the neutrinos themselves. In the limit that neutrinos are free streaming, *i.e.*, outside the neutrinospheres, elastic scattering with electrons is the only neutrino-matter process that is relevant. Of these, the forward scattering amplitudes add coherently with the free propagator to introduce a potential in the flavor evolution Hamiltonian. This contribution due to the net local number density of electrons in the medium is known as the MSW potential [36, 37],

$$\lambda(r) = \sqrt{2}G_F [n_e(r) - n_{e^+}(r)], \quad (9)$$

$$= 6.6 \times 10^5 \text{ km}^{-1} \times \left[ \frac{n_e(r) - n_{e^+}(r)}{10^{33}/\text{cm}^3} \right], \quad (10)$$

where, in the second line, we have used the value of the Fermi constant  $G_F = 1.16 \times 10^{-5} \text{ GeV}^{-2}$ . The matter-induced contribution to the Hamiltonian is represented by a vector  $\lambda(r)\mathbf{L}$ , where  $\mathbf{L} = (0, 0, 1)$ .

The above two contributions are well-known, and lead to the traditional paradigm of core-collapse supernova neutrino oscillations based on vacuum oscillations and matter-induced oscillations [83]. However, near the neutrinosphere, neutrino densities are very high, so in addition to ordinary neutrino oscillations due to  $\omega(\epsilon)$  and matter oscillations due to  $\lambda(r)$ , one has appreciable forward scattering of neutrinos and antineutrinos off each other [38]. This leads to another potential, induced by all other neutrinos and antineutrinos, whose value at the neutrinosphere  $R_{\nu_e}$  is given by [38, 52]

$$\mu_{R_{\nu_e}} = \sqrt{2}G_F \Phi_{\nu, \bar{\nu}} \quad (11)$$

$$= 1.1 \times 10^6 \text{ km}^{-1} \quad (12)$$

$$\times \left[ \frac{(10 \text{ km})^2}{R_{\nu_e}^2} \right] \sum_{\nu_i} \left[ \frac{\mathcal{L}_{\nu_i}}{10^{52} \text{ erg/s}} \right] \left[ \frac{10 \text{ MeV}}{\langle \epsilon_{\nu_i} \rangle} \right].$$

The exact quantity that appears here, *i.e.*,  $\Phi_{\nu, \bar{\nu}} = \Phi_{\nu_e} + \Phi_{\bar{\nu}_e} + 4\Phi_{\nu_x}$ , depends on our chosen normalization for the polarization vectors – Eqs. (5) and (6) have the same quantity in the denominator. Altogether, the equations of motion become [52]

$$\frac{d\mathbf{P}(\epsilon, u)}{dr} = + \frac{\omega(\epsilon)\mathbf{B} \times \mathbf{P}(\epsilon, u)}{v_r(u, r)} + \frac{\lambda(r)\mathbf{L} \times \mathbf{P}(\epsilon, u)}{v_r(u, r)} \quad (13)$$

$$+ \mu_{R_{\nu_e}} \frac{R_{\nu_e}^2}{r^2} \left[ \left( \int_0^1 du' \int_0^\infty d\epsilon' \frac{\mathbf{P}(\epsilon', u') - \bar{\mathbf{P}}(\epsilon', u')}{v_r(u', r)} \right) \times \frac{\mathbf{P}(\epsilon, u)}{v_r(u, r)} - \left( \int_0^\infty d\epsilon' (\mathbf{P}(\epsilon') - \bar{\mathbf{P}}(\epsilon')) \right) \times \mathbf{P}(\epsilon, u) \right],$$

$$\frac{d\bar{\mathbf{P}}(\epsilon, u)}{dr} = - \frac{\omega(\epsilon)\mathbf{B} \times \bar{\mathbf{P}}(\epsilon, u)}{v_r(u, r)} + \frac{\lambda(r)\mathbf{L} \times \bar{\mathbf{P}}(\epsilon, u)}{v_r(u, r)} \quad (14)$$

$$+ \mu_{R_{\nu_e}} \frac{R_{\nu_e}^2}{r^2} \left[ \left( \int_0^1 du' \int_0^\infty d\epsilon' \frac{\mathbf{P}(\epsilon', u') - \bar{\mathbf{P}}(\epsilon', u')}{v_r(u', r)} \right) \times \frac{\bar{\mathbf{P}}(\epsilon, u)}{v_r(u, r)} - \left( \int_0^\infty d\epsilon' (\mathbf{P}(\epsilon') - \bar{\mathbf{P}}(\epsilon')) \right) \times \bar{\mathbf{P}}(\epsilon, u) \right].$$



Note that neutrinos emitted at angle  $\vartheta_{R_{\nu_e}}$  have a radial velocity,

$$v_r(u, r) = \cos \vartheta(u, r) = \sqrt{1 - u \frac{R_{\nu_e}^2}{r^2}}, \quad (15)$$

and their flavor evolution has been projected onto the radial direction.

To keep our discussion simple, we will often use an effective spherically symmetric description proposed in [52], where all neutrinos are assumed to be emitted at  $45^\circ$  to the nominal neutrinosphere at  $R_{\nu_e}$ . This is often referred to as the single-angle approximation. We will see that there is no flavor change close to the neutrinosphere, thus this choice of a common neutrinosphere merely acts as a boundary condition where we specify our initial states. In this approximation, all neutrinos have a radial velocity

$$v_r(r) = \sqrt{1 - \frac{R_{\nu_e}^2}{r^2}}. \quad (16)$$

The forward scattering amplitudes due to neutrinos and antineutrinos scattering off each other leads to a collective potential,

$$\mu(r) = \mu_{R_{\nu_e}} \times \left( \frac{R_{\nu_e}^2}{r^2} \right) \left( \frac{R_{\nu_e}^2/r^2}{2 - R_{\nu_e}^2/r^2} \right). \quad (17)$$

The potential weakens as  $1/r^4$  at large distances because the fluxes dilute as  $1/r^2$  and there is another approximately  $1/r^2$  suppression from the last term in brackets, because the neutrino flux becomes more collinear at large distances. The potential enters the Hamiltonian as  $v_r \mu(r) \mathbf{D}$ , where

$$\mathbf{D} = \int_0^\infty d\epsilon (\mathbf{P}(\epsilon) - \bar{\mathbf{P}}(\epsilon)). \quad (18)$$

Note that the Hamiltonian now depends on  $\mathbf{P}$  and  $\bar{\mathbf{P}}$  themselves, thus making the flavor evolution nonlinear.

The single-angle equations of motion for the flavor composition of neutrino and antineutrino fluxes from a core-collapse supernova are then given by

$$\frac{d\mathbf{P}(\epsilon)}{dr} = \left( +\frac{\omega(\epsilon)\mathbf{B}}{v_r} + \frac{\lambda(r)\mathbf{L}}{v_r} + \mu(r)\mathbf{D} \right) \times \mathbf{P}(\epsilon), \quad (19)$$

$$\frac{d\bar{\mathbf{P}}(\epsilon)}{dr} = \left( -\frac{\omega(\epsilon)\mathbf{B}}{v_r} + \frac{\lambda(r)\mathbf{L}}{v_r} + \mu(r)\mathbf{D} \right) \times \bar{\mathbf{P}}(\epsilon). \quad (20)$$

## B. Flavor Evolution

In the central regions of a core-collapse supernova, the matter potential  $\lambda(r) \gg \omega$ , and the mixing angle  $\theta_{13}$  is suppressed by the factor  $\sim \omega/\lambda$  [36, 37]. As was shown in [47, 49, 54], the role of a large MSW potential is

mimicked by setting the mixing angle  $\theta_{13}$  to a small value, and removing  $\lambda(r)$  from the equations of motion. We use this result without proof. Now, adding Eq. (19) and Eq. (20) and integrating over all energies, one finds that the vector  $\int_0^\infty d\epsilon (\mathbf{P} + \bar{\mathbf{P}}) - \frac{\tilde{\omega}/v_r}{\mu} \mathbf{B}$  acts like a pendulum with the energy [49, 50]

$$E = \frac{\tilde{\omega}}{v_r} \mathbf{B} \cdot \int_0^\infty d\epsilon (\mathbf{P} + \bar{\mathbf{P}}) + \frac{1}{2} \mu(r) |\mathbf{D}|^2, \quad (21)$$

where  $\tilde{\omega}$  is the the average of the oscillation frequency  $\omega$  over the spectrum of flux differences [53],

$$\tilde{\omega} = \frac{\int_0^\infty d\epsilon \omega(\epsilon) \left( \frac{d\Phi_{\nu_e}}{d\epsilon} - \frac{d\Phi_{\nu_x}}{d\epsilon} \right)}{2(\Phi_{\nu_e} - \Phi_{\nu_x})} + \frac{\int_0^\infty d\epsilon \omega(\epsilon) \left( \frac{d\Phi_{\bar{\nu}_e}}{d\epsilon} - \frac{d\Phi_{\bar{\nu}_x}}{d\epsilon} \right)}{2(\Phi_{\bar{\nu}_e} - \Phi_{\bar{\nu}_x})}, \quad (22)$$

and  $\mathbf{B}$  is approximately equal to  $\mp(0, 0, 1) + \mathcal{O}(\theta_{13}^2)$ .

The dynamics of the neutrino flavor pendulum is approximately determined by a comparison of the potential and kinetic energy of the system [49]. The potential energy of the system is the first term on the r.h.s. of Eq. (21), *i.e.*,  $\tilde{\omega} \mathcal{F}_+ / v_r$ , where

$$\mathcal{F}_+ \equiv \mathbf{B} \cdot \int_0^\infty d\epsilon (\mathbf{P} + \bar{\mathbf{P}}), \quad (23)$$

which is initially

$$\mathcal{F}_+(R_{\nu_e}) = \mp \frac{\Phi_{\nu_e} + \Phi_{\bar{\nu}_e} - 2\Phi_{\nu_x}}{\Phi_{\nu_e} + \Phi_{\bar{\nu}_e} + 4\Phi_{\nu_x}}, \quad (24)$$

is the measure of the fraction of the neutrino flux available for oscillation. We remind the reader that the  $\mp$  sign depends on whether  $\Delta m_{\text{atm}}^2 > 0$  (normal hierarchy) or  $< 0$  (inverted hierarchy). On the other hand, the kinetic energy of the system is the second term on the r.h.s. of Eq. (21), given by  $\frac{1}{2} \mu(r) \mathcal{F}_-^2$ , where

$$\mathcal{F}_- \equiv |\mathbf{D}|, \quad (25)$$

which is initially

$$\mathcal{F}_-(R_{\nu_e}) = \frac{\Phi_{\nu_e} - \Phi_{\bar{\nu}_e}}{\Phi_{\nu_e} + \Phi_{\bar{\nu}_e} + 4\Phi_{\nu_x}}, \quad (26)$$

is the net lepton asymmetry in the system. For the first few 100 ms after bounce, in which the explosion mechanism must operate, one typically has  $\Phi_{\nu_e} > \Phi_{\bar{\nu}_e} > \Phi_{\nu_x}$ , thus  $\mathbf{P}_z$  and  $\bar{\mathbf{P}}_z$  are positive except at the very highest energies. For normal hierarchy, *i.e.*,  $\Delta m_{\text{atm}}^2 > 0$ , the potential energy  $\tilde{\omega}/v_r \mathbf{B} \cdot \int_0^\infty d\epsilon (\mathbf{P} + \bar{\mathbf{P}})$  is already negative in the initial state, and therefore the pendulum remains close to its initial state (any other configuration would have higher energy). In the inverted hierarchy, *i.e.*,  $\Delta m_{\text{atm}}^2 < 0$ , however, the potential energy is

positive initially, and flipping the polarization vectors  $\mathbf{P}$  and  $\bar{\mathbf{P}}$  leads to a lowering of the total energy. This instability of the neutrino flavor distribution leads to almost complete flavor conversions by flipping the polarization vectors  $\mathbf{P}$  and  $\bar{\mathbf{P}}$  if  $\Delta m_{\text{atm}}^2 < 0$ .

The above argument assumes that all  $\mathbf{P}_z$  and  $\bar{\mathbf{P}}_z$  are positive, which is true for supernova neutrino fluxes in the early postbounce phase, at all but the very highest energies. This may not always be the case and it is worth emphasizing that even for normal hierarchy it is possible to get flavor flips, as first shown in [60]. However, that requires a larger flux of  $\mu$  and  $\tau$  neutrinos (to make  $\mathbf{P}_z$  and  $\bar{\mathbf{P}}_z$  negative) than is typically available in the early postbounce phase.

When the kinetic energy  $\frac{1}{2}\mu(r)\mathcal{F}_-^2$  becomes comparable to the potential energy  $\tilde{\omega}\mathcal{F}_+/v_r$ , the flavor pendulum begins flipping back and forth between the up and down states, and does not always return to its initial position. This radius, below which the collective potential pins all polarization vectors together and the motion is synchronized, is given by the condition

$$\mu(r_{\text{sync}}) \approx 4\tilde{\omega} \left(1 + \frac{R_{\nu_e}^2}{4r_{\text{sync}}^2}\right) \frac{\mathcal{F}_+}{\mathcal{F}_-^2}. \quad (27)$$

Beyond this radius, the neutrinos begin to convert flavor as the flavor pendulum tends to drift towards the lower energy configuration.

As the neutrinos stream out, the magnitudes of the vacuum Hamiltonian  $\tilde{\omega}/v_r$  and the collective Hamiltonian  $\mu|D|$  eventually become comparable. This happens at a radius  $r_{\text{end}}$  where  $\mu(r_{\text{end}}) \approx \tilde{\omega}(1 + R_{\nu_e}^2/(4r_{\text{end}}^2))/\mathcal{F}_-$ , the flavor pendulum settles into the lower energy state, which involves a flip in flavor space in the inverted hierarchy. Collective flavor conversions approximately freeze-out at this radius. Vacuum and MSW neutrino oscillations take place at much larger radii and we neglect them here.

The flip of the flavor pendulum, as described above, leads to a swap of the  $\nu_e$  and  $\bar{\nu}_e$  number fluxes with those of  $\nu_x$  and  $\bar{\nu}_x$  number fluxes via pair-conversions  $\nu_e\bar{\nu}_e \leftrightarrow \nu_x\bar{\nu}_x$ . The number fluxes after collective effects (on the l.h.s.) are given in terms of the number fluxes before collective effects (on the r.h.s.) as

$$d\Phi_{\nu_e}/d\epsilon = \begin{cases} d\Phi_{\nu_e}/d\epsilon & \epsilon < \epsilon_{\text{split}} \\ d\Phi_{\nu_x}/d\epsilon & \epsilon > \epsilon_{\text{split}} \end{cases}, \quad (28)$$

$$d\Phi_{\bar{\nu}_e}/d\epsilon = d\Phi_{\nu_x}/d\epsilon, \quad (29)$$

$$4d\Phi_{\nu_x}/d\epsilon = d\Phi_{\nu_e}/d\epsilon + d\Phi_{\bar{\nu}_e}/d\epsilon + 2d\Phi_{\nu_x}/d\epsilon, \quad (30)$$

where  $\epsilon_{\text{split}}$  is given by the constraint [51]

$$\int_0^{\epsilon_{\text{split}}} d\epsilon d\Phi_{\nu_e}/d\epsilon = \int_0^\infty d\epsilon (d\Phi_{\nu_e}/d\epsilon - d\Phi_{\bar{\nu}_e}/d\epsilon). \quad (31)$$

The sharp discontinuity for  $\nu_e$  at  $\epsilon_{\text{split}}$  is known in the literature as a spectral split, and appears at  $\sim(6-8)$  MeV. There is a spectral split in  $\bar{\nu}_e$  too,

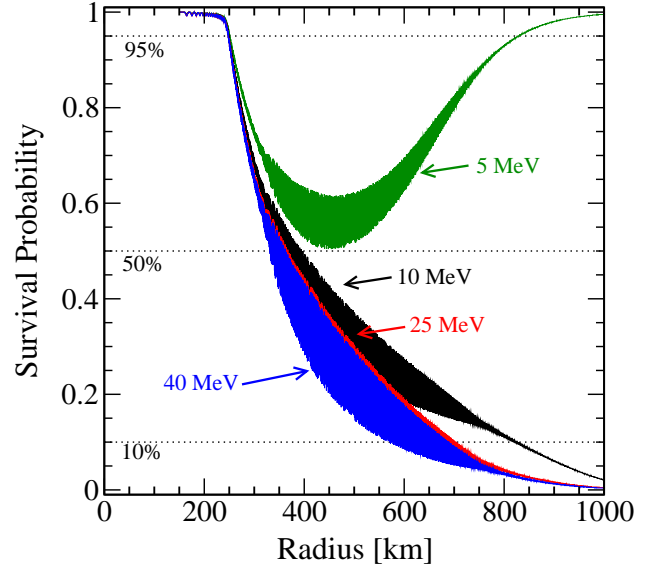


FIG. 1: Survival probabilities of flavor states  $\nu_e$  (same for  $\nu_x$ ) at representative energies (5, 10, 25, and 40 MeV) as a function of distance from the origin in a snapshot at 250 ms after bounce in the core collapse evolution of the  $15-M_\odot$  progenitor star discussed in Section IV A.

but typically at even lower energies ( $< 5$  MeV) and is generally ignored [53, 60].

A representative example of  $\nu_e$  flavor evolution is shown in Fig. 1. Note how the survival probability is initially close to one ( $\nu_e$  preserve their original state), begins to decrease from  $r_{\text{sync}}$  (which in the example shown here is  $\sim 250$  km), and finally around  $r_{\text{end}}$  (here  $\sim 700$  km) asymptotes to zero (complete flavor conversion). Note that there are neutrinos that return back to their original state – those are the lowest energy  $\nu_e$  (below  $\sim 7$  MeV) that do not convert flavor as mentioned above. We remind that in a two-flavor approximation, this survival probability for  $\nu_e$  is exactly the same as for  $\nu_x$ . The behavior of  $\bar{\nu}_e$  (and  $\bar{\nu}_x$ ) is only slightly different (energies below  $\sim 4$  MeV return back to their original flavor), and therefore not shown.

The value of the collective potential when the flavors flip start occurring, *i.e.*,  $\mu(r_{\text{sync}}) = 4\tilde{\omega}(1 + R_{\nu_e}^2/(4r_{\text{sync}}^2))\mathcal{F}_+/\mathcal{F}_-^2$ , does not depend on the total neutrino number flux, but only on the relative number fluxes. Note that  $\Phi_{\nu,\bar{\nu}}$  in  $\mu(r)$  cancels with the denominator of  $\mathcal{F}_-$ , and is simply a choice of normalization. With our normalizations for  $\mathbf{P}$ ,  $\bar{\mathbf{P}}$ , and  $\mu(r)$ , all model-dependence on neutrino spectra is absorbed into one number, *i.e.*,  $\tilde{\omega}\mathcal{F}_+/\mathcal{F}_-^2$ .

For core-collapse supernova emission parameters predicted by typical simulations,  $\tilde{\omega}\mathcal{F}_+/\mathcal{F}_-^2$  is typically in the range  $(30 - 300) \text{ km}^{-1}$ . We plot in Fig. 2, the synchronization radius  $r_{\text{sync}}$  as a function of the number luminosity  $\mathcal{N}_{\nu,\bar{\nu}}$  and the neutrinosphere radius  $R_{\nu_e}$  using Eq. (27) and assuming  $\tilde{\omega}\mathcal{F}_+/\mathcal{F}_-^2 = 50 \text{ km}^{-1}$ . Note that a factor of six increase in the value chosen as the

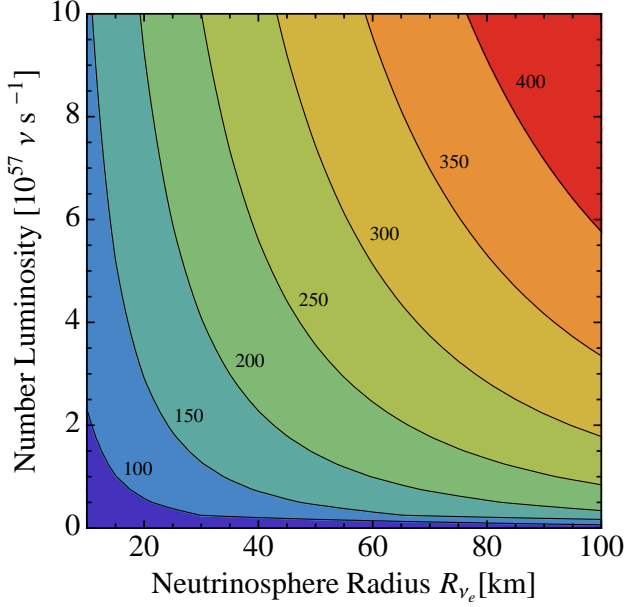


FIG. 2: Contours of equal synchronization radius (in km), using Eq. (27), as a function of the neutrino number luminosity  $\mathcal{N}_{\nu,\bar{\nu}} = 4\pi R_{\nu_e}^2 \Phi_{\nu,\bar{\nu}}$  (in  $10^{57} \text{ s}^{-1}$ ) and the  $\nu_e$  neutrinosphere radius  $R_{\nu_e}$  for a fiducial value of  $\tilde{\omega}\mathcal{F}_+/\mathcal{F}_-^2$  taken to be  $50 \text{ km}^{-1}$ . See text for more details.

critical  $\mu(r_{\text{sync}})$ , reduces  $r_{\text{sync}}$  by only  $\sim 40\%$  because of the  $1/r^4$  scaling of  $\mu$ . In the postbounce pre-explosion phase, the total neutrino number luminosity is  $\mathcal{N}_{\nu,\bar{\nu}} \sim (1-10) \times 10^{57} \text{ s}^{-1}$  and  $\nu_e$  neutrinosphere radius is  $R_{\nu_e} \sim (40-80) \text{ km}$ , which leads to a typical synchronization radius  $r_{\text{sync}} \sim (200-400) \text{ km}$ . Similarly  $r_{\text{end}}$  is seen to be  $\sim (400-700) \text{ km}$ .

Our discussion so far has been based on a single-angle formalism. However, as we have already mentioned, neutrinos emitted at different angles relative to the neutrinosphere experience different collective and MSW potentials. This leads to multi-angle effects. There are three ways in which these multi-angle effects are known to become important.

First, if the MSW potential itself is much larger than the collective potential weighted by the lepton asymmetry factor, *i.e.*,  $\lambda(r)/v_r \gg \mu(r)|\mathbf{D}|$ , collective oscillations are suppressed [58]. Spelled out, this is the case where

$$\lambda(r) \gg 2\sqrt{2}G_F\Phi_{\nu,\bar{\nu}}\frac{R_{\nu_e}^2}{r^2}\mathcal{F}_-. \quad (32)$$

Second, if the  $\nu_e$  and  $\bar{\nu}_e$  fluxes are very similar, *i.e.*,  $\Phi_{\nu_e} \approx \Phi_{\bar{\nu}_e}$ , a single angle treatment is not appropriate due to multi-angle decoherence [52]. In this case, one finds that different angular modes accrue random phases for both normal and inverted hierarchy. Thus the polarization vectors  $\mathbf{P}$  and  $\bar{\mathbf{P}}$  shrink to zero due to kinematic decoherence. This can begin as soon as the synchronization radius is reached and leads to rapid

flavor equilibration (all flavors assume the same spectrum and number flux).

Third, if the fluxes of  $\mu$  and  $\tau$  neutrinos and antineutrinos become comparable to or greater than the  $\nu_e$  or  $\bar{\nu}_e$  fluxes, *i.e.*,  $\Phi_{\nu_x} \gtrsim \Phi_{\nu_e}, \Phi_{\bar{\nu}_e}$ , there can be self-induced suppression of collective oscillations [64]. If this were to happen, it would delay flavor conversions to larger radii. However, in the first few 100 ms after core bounce,  $\Phi_{\nu_x}$  is generally significantly smaller than  $\Phi_{\nu_e}$  and  $\Phi_{\bar{\nu}_e}$ . Hence, self-induced suppression of collective effects, shown to occur when  $\Phi_{\nu_x} \approx \Phi_{\nu_e} \approx \Phi_{\bar{\nu}_e}$  [64], is rather unlikely [53].

We do not have a detailed analytical understanding of these multi-angle effects, and they will be studied numerically in the Section IV C. Before we perform a more detailed numerical study, we can now provide first approximate answers to the two questions raised at the end of Section II.

(i) *What is the typical enhancement in heating that one can expect?* It is easy to see that collective oscillations can give rise to almost *maximal* flavor conversion. All neutrinos and antineutrinos change their spectra, thus the entire  $\nu_e$  and  $\bar{\nu}_e$  spectra can get exchanged with those of  $\nu_x$  leading to the largest possible effect that can be expected from any flavor changing phenomenon. The quantities responsible for heating, *i.e.*,  $\mathcal{L}_{\nu_e}\langle\epsilon_{\nu_e}^2\rangle$  and  $\mathcal{L}_{\bar{\nu}_e}\langle\epsilon_{\bar{\nu}_e}^2\rangle$ , can get replaced by  $\mathcal{L}_{\nu_x}\langle\epsilon_{\nu_x}^2\rangle$ , which may be significantly higher if the luminosities in all flavors are comparable but  $\nu_x$  energies are larger, leading to net enhancement of neutrino heating.

(ii) *Does this enhancement take place at sufficiently small radii to have a significant effect on the total neutrino heating?* Based on typical postbounce neutrino emission characteristics, we expect flavor exchange to begin at  $r_{\text{sync}} \sim (200-300) \text{ km}$  and complete at  $r_{\text{end}} \sim (500-700) \text{ km}$  at  $\sim 100 \text{ ms}$  after bounce. Neglecting multi-angle effects that could force  $r_{\text{sync}} \gtrsim 700 \text{ km}$  [74, 75], the oscillation radii will decrease in the later postbounce evolution, since the neutrinospheres recede and the luminosities decrease with time. Hence, depending on the detailed dynamical evolution of a given core collapse event, collective oscillations may indeed occur at sufficiently small radii to significantly affect neutrino heating. In the next section, we will use full radiation-hydrodynamic core-collapse supernova simulations to obtain a more quantitative handle on the relevance of collective oscillations including multi-angle effects.

#### IV. EFFECT OF COLLECTIVE OSCILLATIONS ON SUPERNOVA SHOCK REVIVAL

To explore the potential effect of collective neutrino oscillations in the core-collapse supernova environment more quantitatively, we perform simulations with VULCAN/2D, an axisymmetric Newtonian radiation-hydrodynamics code [27, 77, 84, 85]. In the variant of VULCAN/2D that we use here, neutrino transport is handled in the multi-group flux-limited diffusion (MGFLD) approximation to the full Boltzmann equation, evolving

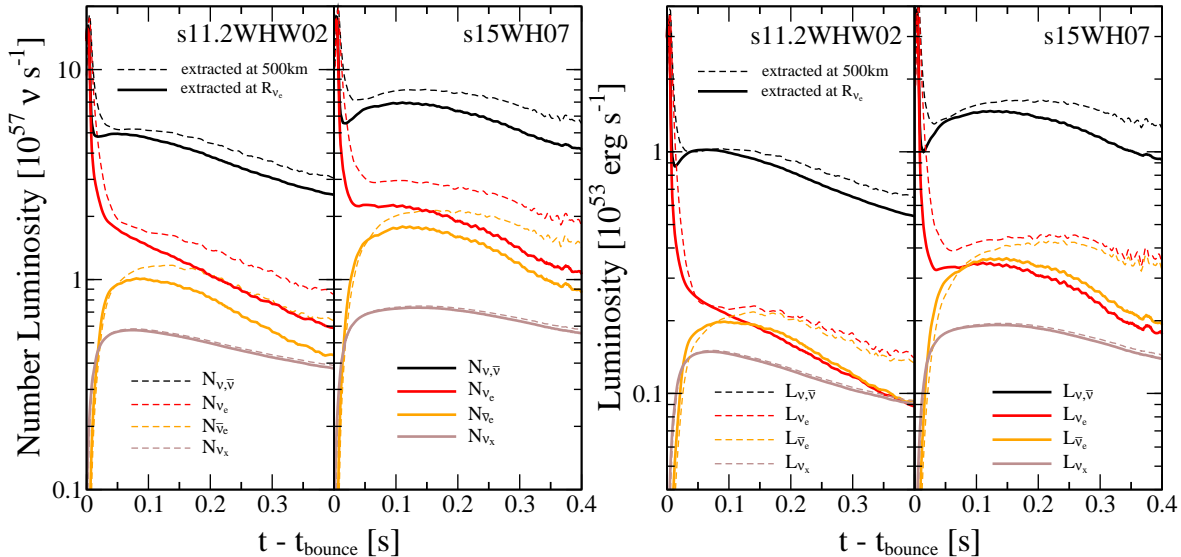


FIG. 3: Neutrino number luminosities (left plot) and energy luminosities (right plot) as a function of time after bounce for model s11.2WHW02 (left panels) and model s15WH07 (right panels). We extract the neutrino luminosities at both the  $\nu_e$  neutrinosphere and at 500 km. The difference in the luminosities between  $R_{\nu_e}$  and 500 km is as expected: little difference in the  $\nu_x$  luminosities but significant differences in the  $\nu_e$  and  $\bar{\nu}_e$  luminosities due to the large accretion luminosity, especially in model s15WH07. We also show the total number luminosity,  $\mathcal{N}_{\nu, \bar{\nu}} = \mathcal{N}_{\nu_e} + \mathcal{N}_{\bar{\nu}_e} + 4\mathcal{N}_{\nu_x}$ , and the total energy luminosity  $\mathcal{L}_{\nu, \bar{\nu}} = \mathcal{L}_{\nu_e} + \mathcal{L}_{\bar{\nu}_e} + 4\mathcal{L}_{\nu_x}$ .

the mean radiation intensity and using Bruenn’s flux limiter [86]. Velocity dependence and energy-redistribution between neutrino groups via inelastic scattering are neglected. Three neutrino species are evolved,  $\nu_e$  and  $\bar{\nu}_e$  along with a representative  $\mu, \tau$  flavor neutrino,  $\nu_x$ , using 16 energy groups, logarithmically spaced from 2.5 to 250 MeV. The neutrino opacities are taken from [87]. More details on VULCAN/2D are provided in [27, 77, 85].

The computational grid consists of an inner quasi-Cartesian region that gradually transitions to an outer polar grid starting at a radius of 20 km and extending out to 5000 km with 221 logarithmically-spaced radial zones and 121 angular zones, covering the full  $180^\circ$  of the axisymmetric domain. Using a Cartesian center avoids the small time steps associated with converging angular zones of a polar grid. See Fig. 4 of [88] for an example of our grid setup.

It is obvious from Fig. 2 that low neutrino number luminosities are favorable for collective oscillations to occur at small radii where they may have an impact on neutrino heating. There is a general trend (at least in the  $\sim (10 - 20)\text{-}M_\odot$  ZAMS mass range) for more massive progenitors to lead to higher postbounce neutrino luminosities [12]. Hence, in this study, we perform calculations with the nonrotating  $11.2\text{-}M_\odot$  progenitor model of Woosley *et al.* [89] (solar composition, model s11.2WHW02 in the following) and, for comparison, also with the nonrotating  $15\text{-}M_\odot$  progenitor model of Woosley & Heger [90] (also solar composition, model s15WH07 in the following).

We evolve both progenitors with the H. Shen *et al.* EOS (HShen EOS, [91, 92]), which is based on a relativistic mean field model of nuclear matter and yields a maximum gravitational mass of  $2.24\text{-}M_\odot$  for a cold neutron star. We follow models s11.2WHW02 and s15WH07 from the onset of core collapse to 400 ms after core bounce and do not observe an onset of explosion in either model before we terminate our calculations. For the  $11.2\text{-}M_\odot$  progenitor, Buras *et al.* [80] observed an early and weak neutrino-driven, SASI-aided explosion. For the  $15\text{-}M_\odot$  progenitor, Bruenn *et al.* reported an explosion setting in at  $\sim 300$  ms after bounce. These differences in outcome observed by these groups may be due to their use of the softest variant of the Lattimer-Swesty EOS [17] (which has now been ruled out [18]), inclusion of general-relativistic effects and/or their more sophisticated treatment of neutrino transport.

#### A. Postbounce Evolution: Neutrino Radiation Fields and Hydrodynamics

In Fig. 3, we show the postbounce neutrino energy luminosities ( $\mathcal{L}_{\nu_i}$ ) and number luminosities ( $\mathcal{N}_{\nu_i}$ ) for models s11.2WHW02 and s15WH07. We extract the angle-averaged luminosities both at the  $\nu_e$  neutrinosphere ( $R_{\nu_e}$ ) and at a radius of 500 km. Significant  $\nu_e$  and, to some extent,  $\bar{\nu}_e$  emission does occur outside the neutrinosphere due to charged-current interactions involving accreted dissociated material (*accretion luminosity*; *e.g.*, [93]). Since the  $\nu_x$  do not participate in charged-current



interactions, their luminosities evolve little between  $R_{\nu_e}$  and 500 km.

In model s15WH07, the neutrino luminosities are consistently higher than in model s11.2WHW02. This is due to the higher temperatures in this progenitor, which lead to higher core luminosities, and to a higher accretion rate, which leads to higher accretion luminosities. With the exception of a very short period close to bounce ( $< 30$  ms), the standard hierarchy of neutrino number flux ( $\Phi_{\nu_i} = \mathcal{N}_{\nu_i}/4\pi r^2$ ),  $\Phi_{\nu_e} > \Phi_{\bar{\nu}_e} > \Phi_{\nu_x}$ , is achieved in both models at  $R_{\nu_e}$  and at 500 km. Such a hierarchy is not present in the energy luminosities at  $R_{\nu_e}$ , but is obtained when taking the accretion luminosity into account.

In the following, we make the simplifying assumption that neutrinos traveling through the neutrinosphere will undergo collective oscillations but those emitted as part of the accretion luminosity will not. This approximation is difficult to overcome, since a full collisional Boltzmann solution including collective oscillations would be required for a self-consistent treatment. However, tests in which we used the asymptotic ( $\mathcal{L}_{\nu_i}^{\text{ns}} + \mathcal{L}_{\nu_i}^{\text{acc}}$ ) instead of the neutrinospheric luminosities led to no qualitative and only small quantitative differences in the critical oscillation radii.

In the left panel of Fig. 4, we show the evolution of the shock radii at the North and South pole, and of the angle-averaged shock radius in model s11.2WHW02. Also shown are the energy-averaged  $\nu_e$  neutrinosphere and gain radii in this model. Until  $\sim 150$  ms after bounce, the shock remains essentially spherically symmetric. Then, the SASI begins to grow and large asymmetries arise in the shock front. The  $\ell = 1$  sloshing of the shock radius in the North-South direction is characteristic of the SASI in 2D (cf. [8], but note that 3D gives a different SASI behavior, *e.g.*, [30]). While oscillations in the shock position reach radii upwards of  $\sim 400$  km, the average peaks at  $\sim 300$  km at  $\sim 150$  ms after bounce, then slowly recedes, reaching  $\sim 200$  km at 350 ms. The angle-averaged gain radius, where charged-current neutrino heating balances cooling, hovers around  $\sim 100$  km. The hashed region denotes the angle-averaged radial extent in which 75% of the net heating occurs. The charged-current interactions are most effective at transferring energy to the matter at high density (cf. Eq. (2)), therefore, most of the net heating occurs near the gain radius where the density is the highest (cf. the discussion in [79] and Fig. 10 of [77] depicting the heating rate as a function of radius). The energy-averaged  $\nu_e$  neutrinosphere radius peaks near  $\sim 70$  km at  $\sim 40$  ms after bounce and recedes thereafter. By 350 ms after bounce, the  $\nu_e$  neutrinosphere has receded to  $\sim 40$  km.

The postbounce evolution of model s15WH07 is summarized by the right panel of Fig. 4. The postbounce dynamics is qualitatively similar to model s11.2WHW02's and quantitative differences are due primarily to model s15WH07's higher postbounce accretion rate. This prevents the shock from reaching the higher radii achieved in model s11.2WHW02 before stagnation and suppresses

the development and the strength of the SASI until later times.

## B. Collective Neutrino Oscillation Radii

Collective neutrino oscillations may be relevant in the postbounce evolution if they occur within the region behind the shock where conditions are conducive to net neutrino heating. We post-process the spectral neutrino fluxes predicted by the VULCAN/2D simulations in two ways to determine the radius at which collective oscillations may begin. As input to these calculations, we chose the neutrino spectra at the  $\nu_e$  neutrinosphere, which we average over lateral angle<sup>1</sup>.

Our first method is using the analytic expressions of Section III. We invert Eq. (27) using Eqs. (17), (22), (24), and (26) and solve for  $r_{\text{sync}}$ ,

$$r_{\text{sync}} = R_{\nu_e} \left[ \frac{1 + \sqrt{2} G_F \Phi_{\nu, \bar{\nu}} / (\tilde{\omega} \mathcal{F}_+ / \mathcal{F}_-^2)}{\sqrt{9 + 8\sqrt{2} G_F \Phi_{\nu, \bar{\nu}} / (\tilde{\omega} \mathcal{F}_+ / \mathcal{F}_-^2) - 1}} \right]^{1/2}. \quad (33)$$

We also use  $\mu(r_{\text{end}}) \approx \tilde{\omega} (1 + R_{\nu_e}^2 / (4r_{\text{end}}^2)) / \mathcal{F}_-$  to obtain an estimate for the radius at which the oscillations effectively are complete. Once again inverting this using Eqs. (17), (26), and (22), we obtain for  $r_{\text{end}}$ ,

$$r_{\text{end}} = R_{\nu_e} \left[ \frac{1 + 4\sqrt{2} G_F \Phi_{\nu, \bar{\nu}} \mathcal{F}_- / \tilde{\omega}}{\sqrt{9 + 32\sqrt{2} G_F \Phi_{\nu, \bar{\nu}} \mathcal{F}_- / \tilde{\omega} - 1}} \right]^{1/2}. \quad (34)$$

As an alternative to the rather rough approximation of Eqs. (33) and (34), we determine the critical collective neutrino oscillation radii by numerically solving the set of coupled nonlinear differential Eqs. (19) and (20) with the initial conditions given by Eqs. (5) and (6) based on the neutrino number fluxes at  $R_{\nu_e}$  in the VULCAN/2D simulations. The equations are solved as a function of radius  $r$  for 32, 64, and 128 energy groups spaced as in Gauss-Legendre quadrature with the oscillation code of Dasgupta *et al.* [54] in combination with the open-source ordinary differential equation solver CVODE [95]. We carry out this calculation for select postbounce times and numerically identify  $r_{\text{sync}}$  and  $r_{\text{end}}$  with the radii at which 5% and 90% flavor conversion have occurred, respectively. For reference, Fig. 1 shows the  $\nu_e$  survival probability for select energies obtained with such an evolution for the neutrino spectra in model s15WH07 at 250 ms after bounce.

We present the results of both methods applied to models s11.2WHW02 and s15WH07 in Fig. 4. The values of  $r_{\text{sync}}$  and  $r_{\text{end}}$  predicted by the two methods agree well at early to intermediate times. At late

<sup>1</sup> Since our models are nonrotating, the variation of the neutrino spectra with lateral angle is not large (cf. [19, 77, 78, 94]).

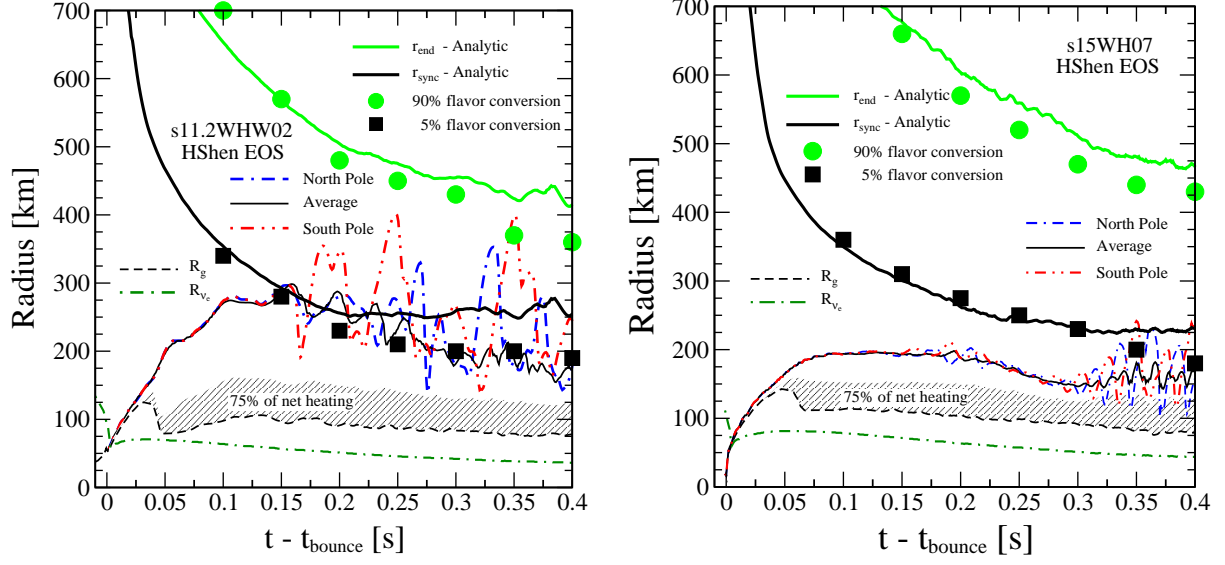


FIG. 4: Comparison of neutrino oscillation radii to shock and gain radii. Average (thin solid lines) and polar shock radii (dot-dot-dashed and dot-dashed-dashed lines) in the postbounce phase of model s11.2WHW02 (left plot) and model s15WH07 (right plot). Also shown (dot-dashed lines) are the energy-averaged  $\nu_e$  neutrinosphere locations and the angle-averaged gain radii (dashed lines). The hashed region just above the gain radius denotes the area in which 75% of the net heating occurs. We show the radii at which collective neutrino oscillations begin ( $r_{\text{sync}}$ ; dark black lines and symbols) and end ( $r_{\text{end}}$ ; light green lines and symbols) as obtained via an analytic approximation (solid lines) and via detailed numerical calculations at select times (squares and circles).  $r_{\text{sync}}$  is initially large, but drops to radii comparable to the shock radii at  $\sim(100 - 150)$  ms in model s11.2WHW02 and at  $\sim(300 - 350)$  ms in model s15WH07. See text for details.

times, the analytic approximation overpredicts by  $\sim 25\%$ . Note that, although the analytical formulae derived in Sec. III B are in a two-flavor approximation, they can be compared to a three-flavor numerical calculation, because the third flavor is almost decoupled.

It is apparent from Fig. 4 that the radial interval over which the collective oscillations occur is well outside the shock at early times. Only after  $\sim 150$  ms ( $\sim 350$  ms) in model s11.2WHW02 (s15WH07), when the total number luminosity has decreased and the neutrinosphere has receded, does  $r_{\text{sync}}$  recede below the shock radius and collective oscillations can have an effect on the subsequent evolution.

### C. Multi-angle Effects

To ascertain the importance of multi-angle effects we use the neutrino luminosities and electron density profile as predicted along the equatorial direction by our VULCAN/2D simulations. Due to the high computational demand of multi-angle oscillation calculations, we do not include the energy spectra of the different flavors, and instead assume a monoenergetic ensemble with the average vacuum oscillation frequency  $\tilde{\omega}$ . This is the same approximation as used by [74, 75]. Since our VULCAN/2D simulations made use of the efficient MGFLD variant of the code, which does not carry direct information on the momentum-space angle dependence

of the neutrino radiation field, we compare with the fully angle-dependent calculations of [77] and construct approximate angle-dependent radiation fields. We find that the angular distribution of the neutrino luminosity, derived from the simulations of [77], is parametrized quite well by  $d\Phi/d\cos\vartheta_{R_{\nu_e}} \propto \exp[(\cos\vartheta_{R_{\nu_e}} - 1)/\sigma_{R_{\nu_e}}]$ , where we choose  $\sigma_{R_{\nu_e}} = 0.357(\langle 1/\mathcal{F} \rangle - 1)$ , and where  $\langle 1/\mathcal{F} \rangle$  is the inverse flux factor. This parameterization reproduces both the isotropic ( $\langle 1/\mathcal{F} \rangle \gg 1$ ,  $\sigma \gg 1$ , and  $d\Phi/d\cos\vartheta \propto \text{constant}$ ) and the free streaming ( $\langle 1/\mathcal{F} \rangle \sim 1$ ,  $\sigma \sim 0$ , and  $d\Phi/d\cos\vartheta \propto \delta(\vartheta)$ ) limits, and qualitatively reproduces the angular distribution at the neutrinosphere (cf. Figure 3 of [77]). At the neutrinosphere, our inverse flux factors are  $\sim 4$ -5. We assume a sharp neutrinosphere, cutting off all neutrinos traveling backwards into the neutrinosphere. With these choices, we solve Eqs. (13) and (14) using a multi-angle oscillation code that is technically similar to the one used for the single-angle calculations.<sup>2</sup>

<sup>2</sup> We have verified numerical convergence by comparing results from calculations with 100, 200, and 400 angular bins. The local error tolerance was fixed at  $10^{-12}$ , which allows us to achieve convergence with  $\sim 400$  modes. Additionally, we have verified the calculations with 800 modes in a limited number of cases, and found them to be consistent. We have also reproduced results similar to Ref.[52].

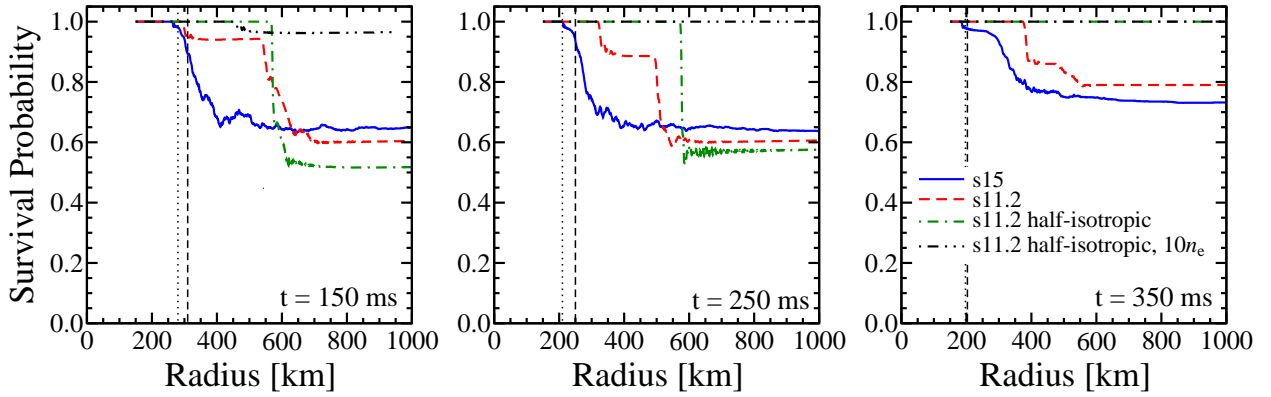


FIG. 5: Survival probabilities (averaged over all emission angles) calculated using a multi-angle oscillation code for a single average energy. The different panels correspond to different times for both models –  $t = 150$  ms (left),  $t = 250$  ms (center), and  $t = 350$  ms (right). Blue solid lines denote results for model s15WH07 and dashed red lines are results for model s11.2WHW02. We also plot results of our cross-checks: dash-dotted green lines are results for model s11.2WHW02 with half-isotropic angular emission and dot-dot-dashed black lines show for the same model the case with half-isotropic angular emission and 10 times higher electron density. The vertical lines are from our *single angle* calculations and represent the radii at which 5% flavor conversion has occurred in models s11.2WHW02 (dotted) and s15WH07 (dashed).

In Fig. 5, we show the survival probability (averaged over all emission angles) of the average-energy neutrinos calculated using the multi-angle code. The three panels show the situation at 150 ms (left), 250 ms (center), and 350 ms (right) after core bounce and results for model s11.2WHW02 and s15WH07 are shown in dashed red and solid blue lines, respectively. The vertical lines in Fig. 5 are from our *single angle* calculations and represent the radii at which 5% flavor conversion has occurred for the s11.2WHW02 (dotted) and the s15WH07 (dashed) progenitors.

We find that in model s11.2WHW02 the onset of flavor conversion is delayed by multi-angle effects to  $\sim (300 - 500)$  km. This is expected and due to high electron number density. As we remarked in Section III, whenever the MSW potential  $\lambda(r) \gg \lambda_{\text{MA}}(r) = 2\sqrt{2}G_F\Phi_{\nu,\bar{\nu}}(R_{\nu_e}^2/r^2)\mathcal{F}_-$ , multi-angle effects are strong and suppress the oscillations. In Fig. 6, we plot  $\lambda(r)$  and  $\lambda_{\text{MA}}(r)$  as a function of radius at 150 ms (left panels), 250 ms (center panels), and 350 ms (right panels) after bounce, for models s11.2WHW02 (top panels) and s15WH07 (bottom panels). Radial profiles along ten lateral directions from the North to South pole are shown to capture variations in  $\lambda(r)$  due to SASI oscillations.  $\lambda(r)$  is almost always larger than  $\lambda_{\text{MA}}$ , which decreases  $\propto r^{-2}$  as expected.  $\lambda(r)$ , which effectively traces the electron number density, falls off  $\propto r^{-3}$  below the shock radius. Above the shock, where matter is essentially in free fall, the density roughly follows  $r^{-1.5}$ . Typically, the ratio  $\lambda(r)/\lambda_{\text{MA}}(r)$  is in the range (1 – 100), getting close to 1 at later times ( $t \gtrsim 250$  ms) at  $r \sim 200$  km in model s11.2WHW02.

Comparing  $\lambda(r)$  along different directions, we find that the SASI oscillations developing at  $t - t_{\text{bounce}} \gtrsim 150$  ms lead to a significant spread in the values of  $\lambda(r)$ ,

sometimes, in model s11.2WHW02, bringing it just below the critical value below which multi-angle suppression is less effective. This occurs when the shock recedes to particularly small radii and the region in which the suppression is lifted is always at or outside the shock.

On the other hand, as we remarked in Section III B, multi-angle effects may appear in a second way: If the  $\nu_e$  and  $\bar{\nu}_e$  fluxes are very similar, *i.e.*,  $\Phi_{\nu_e} \approx \Phi_{\bar{\nu}_e}$ , multi-angle decoherence of flavors sets in. In our model s11.2WHW02, the  $\nu_e$  and  $\bar{\nu}_e$  fluxes are not too similar ( $(\Phi_{\nu_e} - \Phi_{\bar{\nu}_e})/\Phi_{\bar{\nu}_e} \approx 0.25$ ), thus the decoherence effect remains negligible.

In model s15WH07, on the other hand, the multi-angle oscillation calculation does not predict a significant delay in radius compared to the single-angle prediction, in spite of the high electron number density also present in this model. Since in model s15WH07 the  $\nu_e$  and  $\bar{\nu}_e$  fluxes are quite similar ( $(\Phi_{\nu_e} - \Phi_{\bar{\nu}_e})/\Phi_{\bar{\nu}_e} \approx 0.1$ ) early on, we attribute this surprising result to (at least partial) multi-angle flavor decoherence, which leads to oscillations despite the high electron number density. We find flavor conversion almost as soon as the neutrinos cross the synchronization radius. This observation is consistent with the previous work by Esteban-Pretel *et al.*, in which where they found that  $(\Phi_{\nu_e} - \Phi_{\bar{\nu}_e})/\Phi_{\bar{\nu}_e} \lesssim 0.2$  leads to decoherence [52].

Comparing our results quantitatively with the recent multi-angle work of Chakraborty *et al.* [74, 75] is not straightforward, since these authors based their calculations on 1D supernova simulations using a different progenitor model (a  $10.8-M_{\odot}$  progenitor of [89]). However, we note that they observe a stronger multi-angle suppression than borne out by our models. For example, flavor conversion is delayed for their  $10.8-M_{\odot}$  progenitor almost until (700 – 1000) km, while we observe flavor evolution to begin around already at (300 – 500) km in

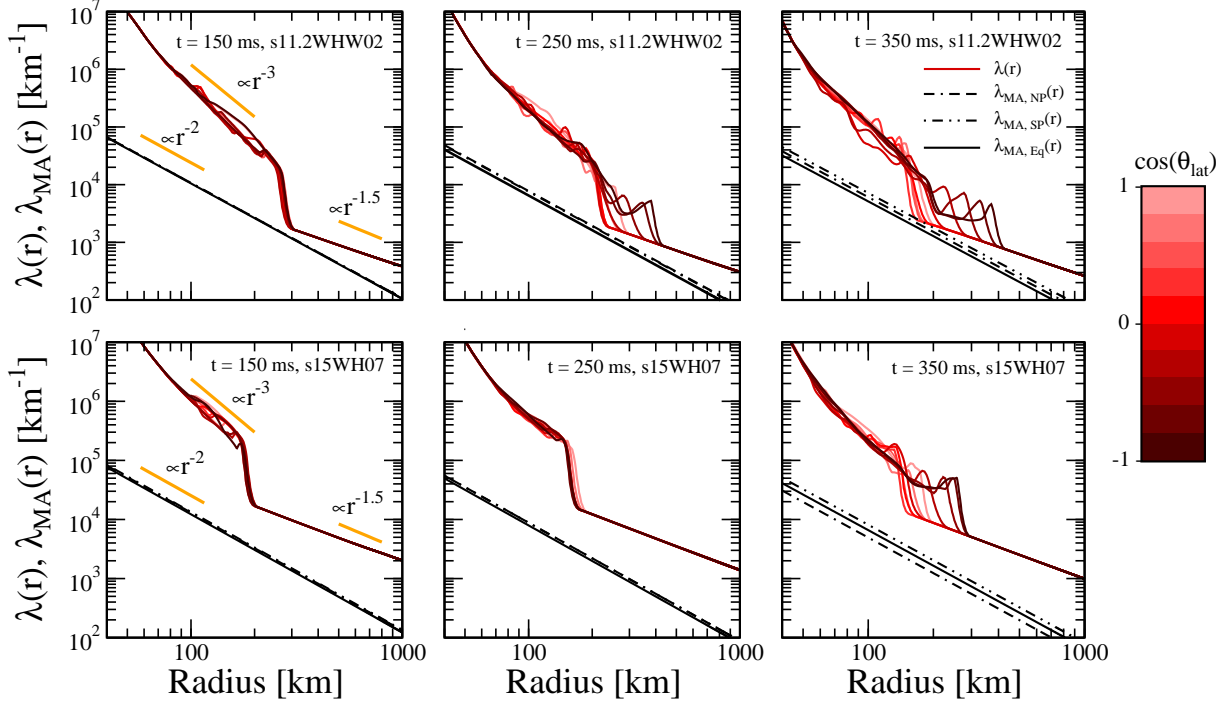


FIG. 6: The MSW potential  $\lambda(r)$  along various directions (thin solid lines, 10 rays equally spaced in  $\cos(\theta_{\text{lat}})$ ), in comparison to the minimum  $\lambda(r)$  needed for multi-angle suppression  $\lambda_{\text{MA}} = 2\sqrt{2}G_F\Phi_{\nu,\bar{\nu}}(R_{\nu_e}^2/r^2)\mathcal{F}_-$  (thick dot-dashed line, taken along the North pole (NP), South pole (SP), and equator (EQ)). To guide the eye, rulers show  $r^{-1.5}$ ,  $r^{-2}$ , and  $r^{-3}$  radial profiles. The steep rise in the  $\lambda(r)$  profiles occurring around  $r \sim 200$  km, but varying with lateral angle, is the location of the shock. The MSW potential  $\lambda(r)$  is generally larger than the critical value  $\lambda_{\text{MA}}(r)$  needed for multi-angle suppression of neutrino oscillations.

our models. We believe that this is due to two reasons:

Firstly, a half-isotropic angular distribution ( $d\Phi/d\cos\vartheta_{R_{\nu_e}} \propto \cos\vartheta_{R_{\nu_e}}$ ) was used in the calculations of [74, 75]. Compared to our angular distribution, this underestimates neutrinos emitted at large angles. The collective interaction is stronger for tangentially emitted neutrinos than for radially emitted neutrinos, therefore suppressing the tangential modes leads to a slower growth of the collective instability. We verify this claim by replacing the angular distribution in our model s11.2WHW02 by a half-isotropic angular distribution. The results for this half-isotropic case are shown in Fig. 5 (dot-dashed green line). The “double-step” feature only appears when we use our angular emission spectrum, which introduces stronger collective effects. This suggests that the feature is related to the angular spectrum, and not a numerical artifact. It is thus clear that simply changing the angular distribution can change the onset of flavor conversion. This may be strong enough to create a qualitative difference as evident from the snapshot at  $t = 350$  ms in our  $11.2-M_\odot$  model, where we find that the oscillations do not occur for a half-isotropic angular distribution, but do occur for our angular distribution modeled after the full 2D multi-angle neutrino transport simulations of [77].

Secondly, in the  $10.8-M_\odot$  model of [74, 75], one

finds a ratio of electron to neutrino density that is up to 10 times larger than in our  $11.2-M_\odot$  model at various radii and times. This is due to the different progenitor structure used – our s11.2WHW02 model has a lower postbounce accretion rate than the models of [74, 75]. We verify that this is indeed an important factor, by artificially increasing the electron density by a factor of 10 and replacing the angular distribution in our oscillation calculations by a half-isotropic angular spectrum for model s11.2WHW02. This case is expected to closely follow the results of [74, 75]. The results of this are shown in Fig. 5 (dot-dot-dashed black line). They demonstrate that such a change in the electron density and angular distribution can indeed significantly suppress the flavor evolution, in agreement with previous results [74, 75].

In the light of these results, we believe that the role of multi-angle effects remains an issue that requires further scrutiny. The role of the matter density,  $\nu_e/\bar{\nu}_e$  asymmetry, and the angular distribution need to be studied in more detail. Flavor conversion are not always completely suppressed due to multi-angle matter suppression. Predictions of the neutrino flavor content at early times must therefore be used with abundant caution. Fortunately, as we shall see in the next section, our conclusions regarding the impact of collective



oscillations on the supernova mechanism remain largely unchanged.

#### D. Potential Enhancement of Neutrino Heating

As discussed in Section III, collective neutrino oscillations (in the inverted mass hierarchy) will lead to a swap of the  $\nu_e$  and  $\bar{\nu}_e$  spectral fluxes with the spectral fluxes of the  $\nu_x$  neutrinos (cf. Eqs. (28)-(30)). In order to illustrate the potential enhancement of neutrino heating due to this swap, we first consider the original heating rate before oscillations (cf. Eq. (3)), which can be expressed as

$$\mathcal{H}_{\text{before}} \sim \hat{\sigma} \langle \epsilon_{\nu_e}^2 \rangle [\mathcal{L}_{\nu_e}^{\text{ns}} + \mathcal{L}_{\nu_e}^{\text{acc}}] c_N + \hat{\sigma} \langle \epsilon_{\bar{\nu}_e}^2 \rangle [\mathcal{L}_{\bar{\nu}_e}^{\text{ns}} + \mathcal{L}_{\bar{\nu}_e}^{\text{acc}}] c_P, \quad (35)$$

where we explicitly split the luminosity into core luminosity emanating from the neutrinosphere ( $\mathcal{L}_{\nu_i}^{\text{ns}}$ ) and accretion luminosity ( $\mathcal{L}_{\nu_i}^{\text{acc}}$ ), the latter being emitted almost entirely interior to the gain region. We take  $\langle \epsilon_{\nu_i}^2 \rangle$  as the value calculated at the  $\nu_e$  neutrinosphere. The  $\nu_x$  do not take part in charge-current interactions and play no role in the heating before oscillations.

We now estimate the heating rate after taking into account a partial conversion of the neutrino spectra in the region behind the shock, as observed at late times in our simulations.

$$\begin{aligned} \mathcal{H}_{\text{after}} \sim \mathcal{H}_{\text{before}} &+ \hat{\sigma} [\langle \epsilon_{\nu_x}^2 \rangle \mathcal{L}_{\nu_x}^{\text{ns}} - \langle \epsilon_{\nu_e}^2 \rangle \mathcal{L}_{\nu_e}^{\text{ns}}] c_N^O \\ &+ \hat{\sigma} [\langle \epsilon_{\nu_x}^2 \rangle \mathcal{L}_{\nu_x}^{\text{ns}} - \langle \epsilon_{\bar{\nu}_e}^2 \rangle \mathcal{L}_{\bar{\nu}_e}^{\text{ns}}] c_P^O \\ &+ \hat{\sigma} \langle \epsilon_{\nu_e}^2 \rangle^* [\langle \epsilon_{\nu_e} \rangle^* (\mathcal{N}_{\nu_e}^{\text{ns}} - \mathcal{N}_{\bar{\nu}_e}^{\text{ns}})] c_N^O. \end{aligned} \quad (36)$$

The stars ( $\star$ ) on  $\langle \epsilon_{\nu_e}^2 \rangle$  and  $\langle \epsilon_{\nu_e} \rangle$  denote that the respective averages are taken over only the part of the spectrum below the split energy  $\epsilon_{\text{split}}$  (cf. Section III).  $c_N^O$  and  $c_P^O$  are the column number densities of interacting baryons taking oscillations into account,

$$c_i^O = \int_{R_g}^{R_s} dr n_i P_{\text{ex}}(r), \quad (37)$$

where  $P_{\text{ex}}(r)$  is the flavor conversion fraction and  $R_g$  and  $R_s$  are the gain and shock radius, respectively. If no oscillations occur,  $P_{\text{ex}} = 0$  everywhere and  $c_i^O$  is zero,  $\mathcal{H}_{\text{after}} = \mathcal{H}_{\text{before}}$ . If complete oscillations occur before  $R_g$ ,  $P_{\text{ex}} = 1$  everywhere and  $c_i^O = c_i$ . All other quantities in Eq. (36) have their pre-oscillated values.

We employ the neutrino data from models s11.2WHW02 and s15WH07 and the analytic approximations to the heating, Eqs. (35) and (36), to calculate the change in the heating rate due to collective oscillations. The column number densities,  $c_i$  and  $c_i^O$ , going into the heating rates are angle-averaged values obtained from simulation data. The results are depicted by Fig. 7. Shown with dashed lines are the

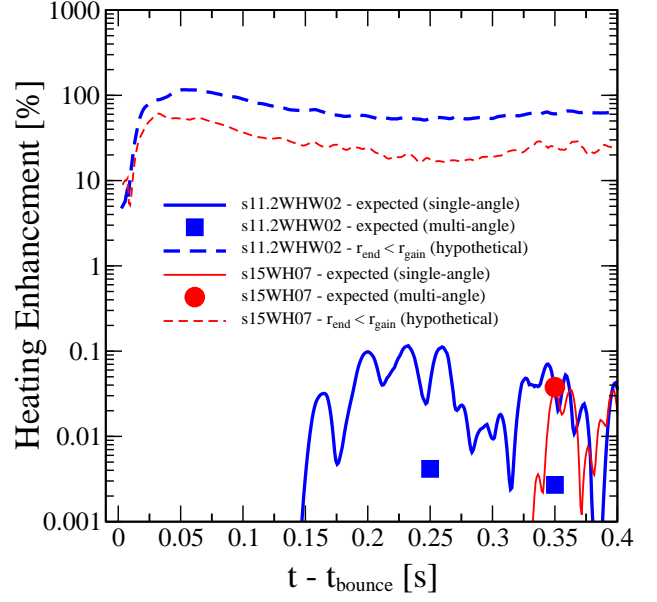


FIG. 7: Time evolution of the potential percentage increase in the heating rate,  $\mathcal{H}_{\text{after}}/\mathcal{H}_{\text{before}} - 1$ , due to collective neutrino oscillation. The dashed lines (thick for model s11.2WHW02 and thin for model s15WH07) assume the hypothetical case of complete conversion already below the gain radius, leading to an enhancement of (20 – 100)% depending on the progenitor and time after bounce. In our simulations, complete conversion does not occur before the gain radius. The more realistic estimate of the heating enhancement based on the oscillation calculations in Section III is much lower and shown in solid lines. Before  $t = 150$  ms and 330 ms the synchronization radius is outside the shock in model s11.2WHW02 and s15WH07, respectively. The points, blue squares for the s11.2WHW02 model and red circles for the s15WH07 model, represent our estimate of the heating enhancement if the multi-angle survival probabilities are used. At 150 ms for the s11.2WHW02 model and at 150 and 250 ms for the s15WH07 model, no heating enhancement is seen, the conversion occurs completely outside the shock.

expected heating enhancements in model s11.2WHW02 (thick lines) and model s15WH07 (thin lines) in a *hypothetical* scenario in which we assume complete flavor conversion *below* the gain radius ( $P_{\text{ex}} = 1$  everywhere). In this extreme case, the heating would be enhanced by  $\gtrsim 60\%$  in model s11.2WHW02 and  $\gtrsim 20\%$  in model s15WH07, this is similar to the configuration of Suwa *et al.* [70]. Note, however, that our assumption that neutrinos of the accretion luminosity do not undergo oscillations may be invalid in this hypothetical situation.

For a more realistic estimate of the heating enhancement, we use  $r_{\text{sync}}$  as numerically computed for both models in Section IV B and assume that above this radius  $P_{\text{ex}} = 0.05$  and below this radius,  $P_{\text{ex}} = 0$ . As a consequence, if  $r_{\text{sync}}$  is greater than the shock radius, there is no heating enhancement. The result of this is shown in Fig. 7 in thick-solid (thin-solid) lines for model s11.2WHW02 (s15WH07). The predicted heating enhancement sets in at much later times and is  $\lesssim 0.1\%$  for

both models. If one instead assumed that  $P_{\text{ex}} = 1$  outside of  $r_{\text{sync}}$ , the enhancement would still be  $\lesssim (2 - 3)\%$

When considering the predicted flavor conversion in our multi-angle calculations discussed in Section IV C, we find, as expected, that there is no further enhancement of the heating, but rather that the enhancement is even more suppressed. We show this in Fig. 7, where we denote by points the expected heating enhancement using the multi-angle survival probabilities presented in Fig. 6 at three postbounce times for each progenitor. In the s11.2WHW02 model, the heating enhancement is zero or reduced significantly. The heating enhancement estimated in the s15WH07 model, where we observed little change in the onset of collective neutrino oscillations, is not as strongly affected. Hence, we conclude that collective neutrino oscillations are very unlikely to have a measurable effect on the neutrino heating and postbounce dynamics in progenitors in and above the mass range considered in this study.

## V. DISCUSSION AND CONCLUSIONS

Almost eight decades after Baade & Zwicky’s stagesetting 1934 proposal [96, 97] that a core-collapse supernova represents the transition of an ordinary star to a neutron star, the details of the mediating mechanism that converts gravitational energy of collapse into energy of the core-collapse supernova explosion remain uncertain.

The neutrino mechanism, based on net heating by charged-current neutrino absorption in the region just below the stalled shock, appears to be the most viable candidate mechanism, requiring the least special conditions (*e.g.*, not requiring rapid rotation or strong magnetic fields etc.) to succeed in exploding garden-variety Type-II supernova progenitor stars. Yet, neutrino-driven explosions fail in 1D, are marginal in 2D simulations, and modeling groups are now exploring the neutrino mechanism’s potentially boosted efficacy in 3D [29, 30]. While dimensionality may be the key to successful explosions, it is also possible that current 1D/2D models are still missing some physics crucial to successful explosions.

In this paper, we have considered new physics previously left out of core-collapse supernova models: collective neutrino flavor oscillations induced by neutrino-neutrino forward scattering in the core-collapse supernova core. If the neutrino mass hierarchy is inverted ( $\Delta m_{\text{atm}}^2 < 0$ ), collective oscillations will invariably lead to a swap of  $\nu_e$  and  $\bar{\nu}_e$  spectra with the significantly harder spectra of their heavy-lepton neutrino counterparts. Assuming a hypothetical scenario in which this swap is complete below the gain region, we find that neutrino heating is enhanced by  $(20 - 100)\%$  in representative Type-II supernova progenitors of  $11.2-M_{\odot}$  and  $15-M_{\odot}$ . Such a significant boost of heating may lead to strong, early explosions, breaking the strong feedback between EOS, weak interactions, neutrino transport, and hydrodynamics that is present in the postbounce phase of

core-collapse supernovae and that tends to absorb small variations in any of its components<sup>3</sup>.

To study the viability of this scenario, we have performed collective neutrino oscillation calculations in the single-angle and multi-angle approximation on the basis of the neutrino radiation fields obtained from 2D neutrino radiation-hydrodynamic core-collapse simulations using  $11.2-M_{\odot}$  and  $15-M_{\odot}$  progenitors. From the oscillation calculations we obtain the characteristic radii  $r_{\text{sync}}$  and  $r_{\text{end}}$  at which  $\sim 5\%$  and  $\sim 90\%$  of the flavor conversion have occurred, respectively. In our simulations, these radii start hundreds of kilometers above the typical shock radii in the early postbounce phase, but recede with time as the neutrinospheres settle to smaller radii as the neutrino luminosities decrease. The radius of onset of oscillations ( $r_{\text{sync}}$ ) reaches the average shock radius at  $(150 - 350)$  ms and thereafter stays close to the latter, while  $r_{\text{end}}$  is systematically  $(150 - 200)$  km outside the average shock radius. As a consequence, most of the flavor conversion occurs outside the shock and can have no effect on the postbounce heating and hydrodynamics. Those oscillations that take place inside the shock occur close to the shock radius and, even when taking large shock excursion driven by the SASI into account, enhance the net heating by less than  $\sim (2 - 3)\%$  in the most optimistic case. These results strongly suggest that collective neutrino oscillations are unlikely to have any qualitative or significant quantitative impact on the postbounce evolution and the explosion mechanism in the standard Type-II supernova progenitors considered here.

Our results also show that the characteristic oscillation radii assume small values faster in cooler, less massive progenitors with lower postbounce accretion rates and smaller neutrinosphere radii in the postbounce phase. While oscillations are unlikely to boost the pre-explosion neutrino heating in our  $11.2-M_{\odot}$  and  $15-M_{\odot}$  models, the situation may be different in even lower-mass progenitors with O-Ne cores or in O-Ne white-dwarf progenitors of accretion induced collapse. The weak explosions already obtained for such progenitors [3–5, 99] could thus be significantly enhanced.

As an aside, we have also shown that the multi-angle matter suppression [58, 74, 75] is somewhat sensitive to the choice of angular emission spectrum and the matter density profile. This is expected to affect the predictions of flavor evolution.

In deriving our results, we have made some approximations and simplifications. Of these the most limiting is that we have assumed a sharp neutrinosphere, common to all flavors and energies. This ignores the interplay of oscillations and collisions, but a completely self-consistent treatment would require a full collisional Boltzmann calculation including oscillations, which must be left to future work. Also, due to computational

<sup>3</sup> This behavior of strongly coupled astrophysical systems is known as *Mazurek’s Law* [98].

limitations, we have not carried out multi-energy multi-angle oscillation calculations, which could be improved upon in subsequent work. The other significant limitation is the assumption of axisymmetry in our supernova calculations. Future, full 3D radiation-hydrodynamics simulations may lead to different hydrodynamic post-bounce evolutions and could yield different results. Given that the understanding of core-collapse supernova physics and collective neutrino oscillations is still in a state of rapid development, there might be additional, yet unknown, effects that could change our conclusions.

Finally, to summarize, collective neutrino oscillations are an intriguing phenomenon. They have important important ramifications for the core-collapse supernova neutrino signature, but, as we have shown in this paper, they develop at too large radii to play a significant role in the explosion mechanism.

### Acknowledgments

We are indebted to E. Livne and A. Burrows for kindly allowing us to use simulation results obtained with VULCAN/2D in this work. Furthermore, we acknowledge helpful discussions with J. Beacom, A. Burrows,

A. Dighe, T. Fischer, E. Livne, O. Pejcha, G. Raffelt, and T. Thompson. BD thanks A. Mirizzi for a useful exchange of preliminary results. CDO wishes to thank M. Kamionkowski for the inspiration to work on this subject and is indebted to P. Vogel for initial discussions and help with neutrino oscillations. BD and CDO would like to thank the organizers of JIGSAW-2010 at TIFR, Mumbai where this project was conceived.

This research is supported in part by the National Science Foundation under grant nos. AST-0855535 and OCI-0905046 and by the Sherman Fairchild Foundation. EOC is supported in part by a post-graduate fellowship from the Natural Sciences and Engineering Research Council of Canada (NSERC).

Results presented in this article were obtained through calculations on the Caltech compute cluster “Zwicky” (NSF MRI award No. PHY-0960291), on the Louisiana Optical Network Initiative supercomputing systems under allocation Ioni\_numrel06, on the NSF TeraGrid under award No. TG-PHY100033, and on resources of the National Energy Research Scientific Computing Center, which is supported by the Office of Science of the U.S. Department of Energy under Contract No. DE-AC02-05CH11231.

- 
- [1] H. A. Bethe and J. R. Wilson, *Astrophys. J.* **295**, 14 (1985).
  - [2] H. A. Bethe, *Rev. Mod. Phys.* **62**, 801 (1990).
  - [3] F. S. Kitaura, H.-T. Janka, and W. Hillebrandt, *A&A* **450**, 345 (2006).
  - [4] L. Hudepohl, B. Müller, H.-T. Janka, A. Marek, and G. G. Raffelt, *Phys. Rev. Lett.* **104**, 251101 (2010).
  - [5] A. Burrows, L. Dessart, and E. Livne, in *AIP Conference Series*, edited by S. Immler and R. McCray (2007), vol. 937, p. 370.
  - [6] M. Liebendörfer, M. Rampp, H.-T. Janka, and A. Mezzacappa, *Astrophys. J.* **620**, 840 (2005).
  - [7] T. A. Thompson, A. Burrows, and P. A. Pinto, *Astrophys. J.* **592**, 434 (2003).
  - [8] J. M. Blondin, A. Mezzacappa, and C. DeMarino, *Astrophys. J.* **584**, 971 (2003).
  - [9] L. Scheck, H.-T. Janka, T. Foglizzo, and K. Kifonidis, *A&A* **477**, 931 (2008).
  - [10] T. Foglizzo, P. Galletti, L. Scheck, and H.-T. Janka, *Astrophys. J.* **654**, 1006 (2007).
  - [11] J. W. Murphy and A. Burrows, *Astrophys. J.* **688**, 1159 (2008).
  - [12] R. Buras, M. Rampp, H.-T. Janka, and K. Kifonidis, *Astron. Astrophys.* **447**, 1049 (2006).
  - [13] A. Marek and H.-T. Janka, *Astrophys. J.* **694**, 664 (2009).
  - [14] O. Pejcha and T. A. Thompson, arXiv:1103.4864 (2011).
  - [15] S. W. Bruenn, A. Mezzacappa, W. R. Hix, J. M. Blondin, P. Marronetti, O. E. B. Messer, C. J. Dirk, and S. Yoshida, in *AIP Phys. Conf. Ser.*, edited by G. Giobbi, A. Tornambe, G. Raimondo, M. Limongi, L. A. Antonelli, N. Menci, and E. Brocato (2009), vol. 1111 of *AIP Phys. Conf. Ser.*, p. 593.
  - [16] Y. Suwa, K. Kotake, T. Takiwaki, S. C. Whitehouse, M. Liebendörfer, and K. Sato, *Pub. Astr. Soc. Jap.* **62**, L49 (2010).
  - [17] J. M. Lattimer and F. D. Swesty, *Nucl. Phys. A* **535**, 331 (1991).
  - [18] P. B. Demorest, T. Pennucci, S. M. Ransom, M. S. E. Roberts, and J. W. T. Hessels, *Nature (London)* **467**, 1081 (2010).
  - [19] A. Marek, H.-T. Janka, and E. Müller, *A&A* **496**, 475 (2009).
  - [20] J. M. LeBlanc and J. R. Wilson, *Astrophys. J.* **161**, 541 (1970).
  - [21] G. S. Bisnovatyi-Kogan, *Astron. Zh.* **47**, 813 (1970).
  - [22] A. Burrows, L. Dessart, E. Livne, C. D. Ott, and J. Murphy, *Astrophys. J.* **664**, 416 (2007).
  - [23] L. Dessart, A. Burrows, E. Livne, and C. D. Ott, *ApJ* **673**, L43 (2008).
  - [24] A. Heger, S. E. Woosley, and H. C. Spruit, *Astrophys. J.* **626**, 350 (2005).
  - [25] C. D. Ott, A. Burrows, T. A. Thompson, E. Livne, and R. Walder, *Astrophys. J. Suppl. Ser.* **164**, 130 (2006).
  - [26] A. Burrows, E. Livne, L. Dessart, C. D. Ott, and J. Murphy, *Astrophys. J.* **640**, 878 (2006).
  - [27] A. Burrows, E. Livne, L. Dessart, C. D. Ott, and J. Murphy, *Astrophys. J.* **655**, 416 (2007).
  - [28] N. N. Weinberg and E. Quataert, *Mon. Not. Roy. Astron. Soc.* **387**, L64 (2008).
  - [29] C. L. Fryer and M. S. Warren, *ApJ* **574**, L65 (2002).
  - [30] J. Nordhaus, A. Burrows, A. Almgren, and J. Bell, *Astrophys. J.* **720**, 694 (2010).
  - [31] S. J. Smartt, *Ann. Rev. Astron. Astrophys.* **47**, 63 (2009).
  - [32] E. O’Connor and C. D. Ott, *Astrophys. J.* **730**, 70 (2011).

- [33] I. Sagert, T. Fischer, M. Hempel, G. Pagliara, J. Schaffner-Bielich, A. Mezzacappa, F. Thielemann, and M. Liebendörfer, *Phys. Rev. Lett.* **102**, 081101 (2009).
- [34] T. Fischer, I. Sagert, G. Pagliara, M. Hempel, J. Schaffner-Bielich, T. Rauscher, F. Thielemann, R. Käppeli, G. Martínez-Pinedo, and M. Liebendörfer, Submitted to *ApJ*, arXiv:1011.3409 (2010).
- [35] B. Pontecorvo, *Sov.Phys.JETP* **26**, 984 (1968).
- [36] L. Wolfenstein, *Phys. Rev.* **D17**, 2369 (1978).
- [37] S. P. Mikheev and A. Y. Smirnov, *Sov. J. Nucl. Phys.* **42**, 913 (1985).
- [38] J. T. Pantaleone, *Phys. Lett.* **B287**, 128 (1992).
- [39] S. Samuel, *Phys. Rev.* **D48**, 1462 (1993).
- [40] V. A. Kostelecky and S. Samuel, *Phys. Rev.* **D52**, 621 (1995).
- [41] S. Pastor, G. G. Raffelt, and D. V. Semikoz, *Phys. Rev.* **D65**, 053011 (2002).
- [42] Y. Y. Y. Wong, *Phys. Rev.* **D66**, 025015 (2002).
- [43] K. N. Abazajian, J. F. Beacom, and N. F. Bell, *Phys.Rev.* **D66**, 013008 (2002).
- [44] A. Friedland and C. Lunardini, *Phys. Rev.* **D68**, 013007 (2003).
- [45] R. F. Sawyer, *Phys. Rev.* **D72**, 045003 (2005).
- [46] G. M. Fuller and Y.-Z. Qian, *Phys. Rev.* **D73**, 023004 (2006).
- [47] H. Duan, G. M. Fuller, and Y.-Z. Qian, *Phys. Rev.* **D74**, 123004 (2006).
- [48] H. Duan, G. M. Fuller, J. Carlson, and Y.-Z. Qian, *Phys. Rev.* **D74**, 105014 (2006).
- [49] S. Hannestad, G. G. Raffelt, G. Sigl, and Y. Y. Y. Wong, *Phys. Rev.* **D74**, 105010 (2006).
- [50] H. Duan, G. M. Fuller, J. Carlson, and Y.-Z. Qian, *Phys. Rev.* **D75**, 125005 (2007).
- [51] G. G. Raffelt and A. Y. Smirnov, *Phys. Rev.* **D76**, 081301 (2007).
- [52] A. Esteban-Pretel, S. Pastor, R. Tomas, G. G. Raffelt, and G. Sigl, *Phys.Rev.* **D76**, 125018 (2007).
- [53] G. L. Fogli, E. Lisi, A. Marrone, and A. Mirizzi, *JCAP* **0712**, 010 (2007).
- [54] B. Dasgupta and A. Dighe, *Phys.Rev.* **D77**, 113002 (2008).
- [55] H. Duan, G. M. Fuller, and Y.-Z. Qian, *Phys. Rev.* **D77**, 085016 (2008).
- [56] B. Dasgupta, A. Dighe, A. Mirizzi, and G. G. Raffelt, *Phys. Rev.* **D77**, 113007 (2008).
- [57] B. Dasgupta, A. Dighe, and A. Mirizzi, *Phys. Rev. Lett.* **101**, 171801 (2008).
- [58] A. Esteban-Pretel, A. Mirizzi, S. Pastor, R. Tomas, G. Raffelt, et al., *Phys.Rev.* **D78**, 085012 (2008).
- [59] J. Gava, J. Kneller, C. Volpe, and G. C. McLaughlin, *Phys. Rev. Lett.* **103**, 071101 (2009).
- [60] B. Dasgupta, A. Dighe, G. G. Raffelt, and A. Y. Smirnov, *Phys. Rev. Lett.* **103**, 051105 (2009).
- [61] B. Dasgupta, G. G. Raffelt, and I. Tamborra, *Phys.Rev.* **D81**, 073004 (2010).
- [62] G. G. Raffelt and I. Tamborra, *Phys.Rev.* **D82**, 125004 (2010).
- [63] J. F. Cherry, G. M. Fuller, J. Carlson, H. Duan, and Y.-Z. Qian, *Phys. Rev.* **D82**, 085025 (2010).
- [64] H. Duan and A. Friedland, *Phys. Rev. Lett.* **106**, 091101 (2011).
- [65] A. Mirizzi and R. Tomas, arXiv:1012.1339 (2010).
- [66] S. Galais, J. Kneller, and C. Volpe, arXiv:1102.1471 (2011).
- [67] G. G. Raffelt, arXiv:1103.2891 (2011).
- [68] Y. Pehlivan, A. Balantekin, T. Kajino, and T. Yoshida, arXiv:1105.1182 (2011).
- [69] H. Duan, G. M. Fuller, and Y.-Z. Qian, *Ann. Rev. Nucl. Part. Sci.* **60**, 569 (2010).
- [70] Y. Suwa, K. Kotake, T. Takiwaki, M. Liebendörfer, and K. Sato, *Astrophys. J.* **738**, 165 (2011).
- [71] G. M. Fuller, R. Mayle, B. S. Meyer, and J. R. Wilson, *Astrophys. J.* **389**, 517 (1992).
- [72] E. K. Akhmedov, A. Lanza, S. Petcov, and D. Sciama, *Phys.Rev.* **D55**, 515 (1997).
- [73] E. Otten and C. Weinheimer, *Rept.Prog.Phys.* **71**, 086201 (2008).
- [74] S. Chakraborty, T. Fischer, A. Mirizzi, N. Saviano, and R. Tomas, arXiv:1104.4031 (2011).
- [75] S. Chakraborty, T. Fischer, A. Mirizzi, N. Saviano, and R. Tomas, arXiv:1105.1130 (2011).
- [76] L. Dessart, A. Burrows, E. Livne, and C. D. Ott, *Astrophys. J.* **645**, 534 (2006).
- [77] C. D. Ott, A. Burrows, L. Dessart, and E. Livne, *Astrophys. J.* **685**, 1069 (2008).
- [78] T. D. Brandt, A. Burrows, C. D. Ott, and E. Livne, *Astrophys. J.* **728**, 8 (2011).
- [79] H.-T. Janka, *A&A* **368**, 527 (2001).
- [80] R. Buras, H.-T. Janka, M. Rampp, and K. Kifonidis, *A&A* **457**, 281 (2006).
- [81] A. Strumia and F. Vissani, arXiv:hep-ph/0606054 (2006).
- [82] T. Schwetz, M. Tortola, and J. Valle, arXiv:1103.0734 (2011).
- [83] A. S. Dighe and A. Y. Smirnov, *Phys.Rev.* **D62**, 033007 (2000).
- [84] E. Livne, *Astrophys. J.* **412**, 634 (1993).
- [85] E. Livne, L. Dessart, A. Burrows, and C. A. Meakin, *ApJS* **170**, 187 (2007).
- [86] S. W. Bruenn, *ApJS* **58**, 771 (1985).
- [87] A. Burrows, S. Reddy, and T. A. Thompson, *Nuclear Physics A* **777**, 356 (2006).
- [88] C. D. Ott, A. Burrows, E. Livne, and R. Walder, *Astrophys. J.* **600**, 834 (2004).
- [89] S. E. Woosley, A. Heger, and T. A. Weaver, *Rev. Mod. Phys.* **74**, 1015 (2002).
- [90] S. E. Woosley and A. Heger, *Phys. Rep.* **442**, 269 (2007).
- [91] H. Shen, H. Toki, K. Oyamatsu, and K. Sumiyoshi, *Nucl. Phys. A* **637**, 435 (1998), URL [http://user.numazu-ct.ac.jp/\\$\sim\\$sumi/eos](http://user.numazu-ct.ac.jp/$\sim$sumi/eos).
- [92] H. Shen, H. Toki, K. Oyamatsu, and K. Sumiyoshi, Submitted to the *Astrophys. J.*, arXiv:1105.1666 (2011).
- [93] T. Fischer, S. C. Whitehouse, A. Mezzacappa, F.-K. Thielemann, and M. Liebendörfer, *A&A* **499**, 1 (2009).
- [94] T. Lund, A. Marek, C. Lunardini, H.-T. Janka, and G. Raffelt, *Phys.Rev.* **D82**, 063007 (2010).
- [95] S. D. Cohen and A. C. Hindmarsh, *Comp. in Phys.* **10(2)**, 138 (1996), URL <https://computation.llnl.gov/casc/sundials>.
- [96] W. Baade and F. Zwicky, *Proc. Nat. Acad. Sci.* **20**, 254 (1934).
- [97] W. Baade and F. Zwicky, *Proc. Nat. Acad. Sci.* **20**, 259 (1934).
- [98] C. D. Ott, E. Schnetter, A. Burrows, E. Livne, E. O'Connor, and F. Löffler, *J. Phys. Conf. Ser.* **180**, 012022 (2009).
- [99] L. Dessart, A. Burrows, C. D. Ott, E. Livne, S.-Y. Yoon, and N. Langer, *Astrophys. J.* **644**, 1063 (2006).